11-3-2016

MSL1 is a mechanosensitive ion channel that dissipates mitochondrial membrane potential and maintains redox homeostasis in mitochondria during abiotic stress

Chun Pong Lee

Grigory Maksaev

Gregory S. Jensen

Monika W. Murcha

Margaret E. Wilson

See next page for additional authors

Authors
Chun Pong Lee, Grigory Maksaev, Gregory S. Jensen, Monika W. Murcha, Margaret E. Wilson, Mark Fricker, Ruediger Hell, Elizabeth S. Haswell, A Harvey Millar, and Lee J. Sweetlove

Received Date : 24-May-2016

Revised Date : 04-Aug-2016

Accepted Date : 05-Aug-2016

Article type : Original Article

MSL1 is a mechanosensitive ion channel that dissipates mitochondrial membrane potential and maintains redox homeostasis in mitochondria during abiotic stress.

Chun Pong Lee*, Grigory Maksaev** Gregory S. Jensen**, Monika W. Murcha*, Margaret E. Wilson**, Mark Fricker***, Ruediger Hell****, Elizabeth S. Haswell**, A. Harvey Millar*, Lee Sweetlove***

* ARC Centre of Excellence in Plant Energy Biology, Bayliss Building M316, University of Western Australia, 35 Stirling Highway, Crawley 6009, Western Australia, Australia

**Department of Biology, Mailcode 1137, Washington University in Saint Louis, One Brookings Drive, Saint Louis, MO, 63130

*** Department of Plant Sciences, University of Oxford, South Parks Road, Oxford, OX1 3RB, UK

**** Department of Plant Molecular Biology, Centre for Organismal Studies, Im Neuenheimer Feld 360, University of Heidelberg, D-69120 Heidelberg, Germany

Corresponding author email id: lee.sweetlove@plants.ox.ac.uk

Short title: A mitochondrial mechanosensitive ion channel

ABSTRACT

Mitochondria must maintain tight control over the electrochemical gradient across their inner membrane to allow ATP synthesis while maintaining a redox-balanced electron transport chain and avoiding excessive reactive oxygen species production. However, there is a scarcity of knowledge about the ion transporters in the inner mitochondrial membrane that contribute to control of membrane potential. We show that loss of MSL1, a member of a family of mechanosensitive ion channels related to the bacterial channel MscS, leads to increased membrane potential of Arabidopsis mitochondria under specific bioenergetic states. We demonstrate that MSL1 localises to the inner mitochondrial membrane. When

expressed in *E. coli*, MSL1 forms a stretch-activated ion channel with a slight preference for anions and provides protection against hypo-osmotic shock. In contrast, loss of MSL1 in Arabidopsis did not prevent swelling of isolated mitochondria in hypo-osmotic conditions. Instead, our data suggest that ion transport by MSL1 leads to dissipation of mitochondrial membrane potential when it becomes too high. The importance of MSL1 function was demonstrated by the observation of a higher oxidation state of the mitochondrial glutathione pool in *msl1-1* mutants under moderate heat- and heavy-metal-stress. Furthermore, we show that MSL1 function is not directly implicated in mitochondrial membrane potential pulsing but is complementary and appears to be important under similar conditions.

INTRODUCTION

The bioenergetic function of mitochondria is crucially dependent on the impermeable nature of their inner membrane to protons such that an electrochemical gradient can be established by the proton-pumping activity of the respiratory chain. This provides the proton motive force (Δp) that powers the F_1F_0ATP synthase. In plant mitochondria, the presence of an active K^+/H^+ exchange across the inner membrane (Hensley and Hanson, 1975; Zotova et al., 2010) means that ΔpH is a relatively minor component of Δp in plant mitochondria (Mitchell and Moyle, 1969; Nicholls, 1974; Santo-Domingo and Demaurex, 2012). In addition to K^+/H^+ exchange, it has long been apparent that plant mitochondrial membranes are permeable to other cations and anions (Moore and Wilson, 1977; Huber and Moreland, 1979; Jung and Brierley, 1979). However, the transporter proteins responsible for these ion fluxes are largely unknown and the purpose of these other ion-transport capabilities has not been established. One possibility is that ion transporters lead to a net transfer of charge from the intermembrane space to the matrix that serves to dissipate mitochondrial membrane potential ($\Delta\Psi_M$) and results in the endogenous inner membrane 'leak' observed in energised mitochondria. This is apparent as continued electron transport (oxygen consumption) in the absence dissipation of ΔpH by F_1F_0ATP synthase and can be stimulated by metals such as cadmium (Kesseler and Brand, 1994b, a, c). While membrane leak is disadvantageous in terms of ATP production it would be beneficial in situations where there is an imbalance between the rate of electron transport / proton pumping and F_1F_0ATP synthase activity, leading to a very high electrochemical potential across the inner membrane. Such an imbalance leads to increased production of damaging reactive oxygen species (ROS) because the large electrochemical gradient makes it harder for the respiratory chain complexes to pump protons against that gradient. Because redox cycling of complexes I, III and IV is coupled to proton pumping, this has the effect of reducing the rate of electron

transport in the respiratory chain. As a result, the respiratory complexes become highly reduced which increases the propensity for ROS production by transfer of single electrons to molecular oxygen (Møller, 2001). Ion transport events that reduce the electrochemical gradient would therefore help prevent ROS production by easing the restriction on respiratory chain electron transport.

One established mechanism in which ion transport process functions in this way is mediated by uncoupling protein (UCP; (Vercesi et al., 2006)) that allows movement of protons from the intermembrane space to the matrix, most likely via an indirect mechanism involving transport of anionic fatty acids (Jezek et al., 1997). UCP is activated under conditions of bioenergetic imbalance (Smith et al., 2004) and has been demonstrated to reduce the production of mitochondrial ROS and to protect against oxidative stress (Barreto et al., 2014). Although activation of UCP is rapid, inactivation probably involves the turnover of the protein (Azzu et al., 2010) and thus UCP can be considered a medium timescale response to persistent mitochondrial imbalance caused by environmental stress. However, to maintain homeostasis there must also be mechanisms that can operate on a short timescale. Rapid, short term dissipation of $\Delta\Psi_M$ has been observed in plant mitochondria with transients (pulses) lasting less than a minute (Schwarzländer et al., 2012). This appears to involve selective cation transport although the transporter or channel responsible has not been identified. Although the first molecular details of regulated cation transport in plant mitochondria are beginning to emerge with the identification of proteins involved in mitochondrial Ca^{2+} transport (Wagner et al., 2015; Wagner et al 2016), it is not yet clear if these proteins are involved in bioenergetic balancing. More work needs to be done to fully understand the mechanisms of ion transport in plant mitochondria and the biochemical and physiological roles of the transport events.

To this end, we searched for putative mitochondrial transporter proteins in Arabidopsis based on sequence analysis (identification of a mitochondrial targeting peptide and presence of extensive hydrophobic domains of sufficient length to be membrane spanning). One of the proteins we identified is a member of the MscS-Like (MSL) family of mechanosensitive ion channels (At4g00290; MSL1 (Hamilton et al., 2015a)). This ten-member gene family was initially identified in Arabidopsis based on homology with the bacterial mechanosensitive ion channel of small conductance MscS (Pivetti et al., 2003). The MSL proteins have different subcellular locations and have been identified or predicted to localise to the plasma membrane, ER and plastid, with MSL1 being the only member with a putative mitochondrial localisation (Hamilton et al., 2015a). Like their bacterial homologs, the MSL proteins

characterized to date can be stretch-activated ion channels and show a slight preference for anions (Maksaev and Haswell, 2012; Hamilton et al., 2015b). In bacteria, stretch-activation of MscS promotes survival of hypo-osmotic shock: opening of the channel following cell swelling leads to the release of ions, reducing the cell's osmotic potential (Levina et al., 1999). A similar hypo-osmotic shock protection role within plastids and during pollen germination has been demonstrated for specific Arabidopsis MSL family members (Veley et al., 2012; Hamilton et al., 2015b). Nevertheless, MSL proteins also appear to have other functions in plants including control of plastid division (Haswell and Meyerowitz, 2006; Wilson et al., 2011) and activation of programmed cell death by the plasma membrane-localised MSL10 (Veley et al., 2014). In this paper, we present a characterisation of the localisation and electrophysiological properties of MSL1 and investigate the conditions under which it is important for bioenergetics homeostasis.

RESULTS

MSL1 is an integral membrane protein in the mitochondrion

Among the ten MSL genes that harbour a conserved MscS domain in Arabidopsis, only MSL1 has a consensus mitochondrial class II (-3 R) cleavage site at Phe-79 (RAF↓SS; (Huang et al., 2009)). It is also the MSL family member that has been identified by previous proteomic analyses in either mitochondria- or plastid-enriched fractions (Froehlich et al., 2003; Zybailov et al., 2008; Ferro et al., 2010; Klodmann et al., 2011; Nikolovski et al., 2012), raising the possibility that MSL1 may be dual-targeted. To clarify the subcellular localization of MSL1, a C-terminal MSL1-GFP fusion was expressed under the control of the 35S promoter in transgenic Arabidopsis plants. Confocal laser scanning microscope (CLSM) imaging of leaf epidermal cells in this transgenic line revealed that MSL1-GFP localized to subcellular structures resembling mitochondria (Figure 1A). MSL1-GFP co-localized with the mitochondrial marker MitoTracker Red in root hair cells (Figure 1B), confirming a mitochondrial localization. To further verify MSL1 localization, an *in vitro* import assay was carried out by incubating radiolabelled precursor MSL1 with isolated mitochondria under conditions that support import (Figure 1C). MSL1 was imported into a proteinase K-resistant location inside mitochondria. Import required a negative mitochondrial membrane potential, as evidenced by the lack of proteinase K-protected mature MSL1 in the presence of valinomycin (Figure 1C). The presence of a processing intermediate and a mature protein indicate that MSL1 is most likely imported via a two-step process common to the import of inner membrane proteins that contain a cleavable pre-sequence (Murcha et al., 2004). In

contrast, MSL1 is not imported into chloroplasts *in vitro* (Supplementary Figure 1), providing additional evidence that MSL1 is exclusively localized to mitochondria.

MSL1 is reported to be uniformly expressed across tissue types and developmental stages, as well as under most biotic and abiotic treatments (Genevestigator and AtGenExpress Visualization Tool analysis). To analyse the physiological and functional relevance of MSL1 in plant, we isolated a homozygous T-DNA insertion line (*msl1-1*) that carries a T-DNA insertion in the first exon leading to an absence of *MSL1* transcript (Supplementary Figure 2A, B). A homozygous *msl1-1* line complemented with a construct containing the genomic version of *MSL1* controlled by its native promoter was also generated (*msl1-1*/*gMSL1*; Supplementary Figure 2B, C). Both transgenic lines show similar growth and morphology to wild type plants under standard growth conditions on agar plates and on soil (Supplementary Figure 2D). Using these genetic resources we confirmed that a peptide antibody raised against the C-terminal end of MSL1 was specific for this protein (Supplementary Figure 2C). We then further used this antibody to assess the precise intra-mitochondrial localization and orientation of MSL1. Based on the consensus TM prediction algorithms in ARAMEMNON (Schwacke et al., 2003), MSL1 is probably comprised of five transmembrane helices. When isolated mitochondrial membranes were fractionated into carbonate-soluble (peripheral) and -insoluble (integral) membrane proteins and analysed by Blue-Native PAGE and immunoblotting, MSL1 could only be found in the integral membrane fraction and migrated as a large ~350 kDa oligomeric complex (after correction by a factor of 0.7 for digitonin and Coomassie binding (Wittig et al., 2010)) (Figure 1D). The immuno-reactive protein band on Blue-Native PAGE was confirmed to be MSL1 by analysis of trypsin-digest-peptides using mass spectrometry (Supplementary Data 1). Furthermore, no trypsin-cleavable peptide fragments preceding Ser-83 (i.e. the mitochondrial targeting sequence) were detected (Supplementary Data 1), suggesting that MSL1 is imported into the mitochondrial matrix where its pre-sequence is cleaved before it is inserted, most likely, into the inner membrane. To test this, we assessed the accessibility of MSL1 to degradation by proteinase K in inner membrane vesicles lacking the outer membrane (mitoplasts) by immuno-blotting of MSL1 and marker proteins. Successful preparation of outer membrane-free mitoplasts was confirmed by the absence of the voltage-dependent anion channel (VDAC, outer membrane) and the sensitivity of cytochrome c (intermembrane space) to degradation by proteinase K (Figure 1E). Both an MSL1-containing complex and the inner membrane protein SLP2 (Gehl et al., 2014) were detected in the mitoplast fraction treated with proteinase K (Figure 1E). The detection of MSL1 band by anti-MSL1 antibodies, which recognize a short hydrophilic peptide sequence near the C-terminal end of MSL1 (see Materials and Methods), indicates

that this region of the protein is in the matrix and is not accessible to proteinase K. In summary, MSL1 is an integral inner membrane protein of mitochondria with the C-terminus orientated towards the matrix.

MSL1 activity is a stretch-activated ion channel

To establish if MSL1 forms a mechanosensitive (MS) ion channel we used single-channel patch clamp electrophysiology. An N-terminal 6xHis-*AtMSL1* construct was expressed in an *E. coli* strain that lacks all seven known mechanosensitive ion channels (MJF641, Δ7, (Edwards et al., 2012)) to provide an electrophysiologically-silent background. When expressed in *E. coli*, the 6xHis-tagged mature MSL1 (lacking its predicted mitochondrial targeting peptide) can be found in the total soluble fraction (Supplementary Figure 3A) and forms a large complex with a similar oligomeric size to the mitochondrial MSL1 (Supplementary Figure 3B; Figure 1D). Giant *E. coli* spheroplasts expressing mature MSL1 produced ion channel activity in response to increased lateral membrane tension, applied as suction—or negative pressure—through the patch pipette (Figure 2A).

The current/voltage plot for MSL1 gated by tension between +40 to -180 mV (Figure 2B) reveals that at negative membrane potentials, MSL1 has a single channel conductance of 1.2 nS. This is the same single channel conductance observed for *E. coli* MscS in the same system (Booth et al., 2011; Kung et al., 2010). However, MSL1 activity in *E. coli* spheroplasts was less stable than MscS, alternating more frequently between conducting and non-conducting states. MSL1 is likely to be oriented in the *E. coli* plasma membrane the same way as MscS, with the C-terminus facing the cytoplasm (Miller et al., 2003). MSL1 is similarly oriented in the inner membrane of mitochondria, with the C-terminus in the matrix (Figure 1). Both the *E. coli* plasma membrane and the mitochondrial inner membrane have strongly negative membrane potentials, indicating that MSL1 is likely to have high conductance in mitochondria once it is gated by membrane tension. Even in the absence of applied tension, we routinely observed noisy activity that may represent MSL1 channel opening at strongly negative membrane potentials (-160 mV or higher, double asterisk in Figure 2C). However, the membranes of *E. coli* giant spheroplasts deteriorate under such high membrane potentials, and it is therefore formally possible that this activity represents current fluctuation associated with imminent patch rupture (arrow, Figure 2C). We occasionally (in about 20% of patches) observed more easily identified opening and closing events without added tension at moderate membrane potentials (-60 to -100 mV, single

asterisk, Figure 2C), suggesting that MSL1 may be voltage-gated, although it remains possible that this activity may be a response to transient fluctuations in patch tension. At positive membrane potentials, which are not physiologically relevant for *E. coli* or for the inner mitochondrial membrane, MSL1 channel activity was reduced and unstable (Supplementary Figure 4).

The anion preference of MSL1 was found to be very mild (Figure 2D), with a reversal potential (E_{rev}) of 10.2 mV and a preference for anions over cations (P_{Cl} : P_K) by a factor of ~2.2. These characteristics closely resemble those reported previously for *Ec*MscS under the same experimental conditions in giant spheroplasts (E_{rev} = 9.5 mV, (Edwards et al., 2008), E_{rev} = 12 mV, (Li et al., 2002)) and when *Ec*MscS was reconstituted into the liposomes (P_{Cl} : P_K = 1.5, (Sukharev, 2002)), P_{Cl} : P_K = 2.7 (Cox et al., 2013)). These results indicate that MSL1 is essentially non-selective and when open allows the passage of small anions and cations with similar efficiency.

MSL1 can provide modest protection against hypo-osmotic shock in *E. coli* but not in plant mitochondria

In bacteria, MscS protects against hypo-osmotic shock; the increased membrane tension due to cell swelling causes stretch-activated opening of the channel and release of ions, reducing the osmotic potential of the cell (Naismith and Booth, 2012). To determine if MSL1 was similarly capable of protecting bacterial cells from hypo-osmotic shock, MSL was expressed in the *E. coli* strain MJF465 that lacks three key mechanosensitive ion channels, MscS, MscL, and MscK (Levina et al., 1999). As expected, MJF465 cells do not survive severe hypo-osmotic shock, but this sensitivity could be fully rescued by expressing MscS from an IPTG-inducible plasmid (Figure 3A). Inducible expression of MSL1 resulted in partial rescue (40% of wild type survival) of the MJF465 osmotic shock sensitivity. Similar results were previously obtained for MSL3, a plastid-localized MscS homolog also from Arabidopsis (Haswell and Meyerowitz, 2006). To establish if MSL1 fulfils a similar osmotic-shock protection role in plant mitochondria, we examined the hypo-osmotic swelling behaviour of mitochondria isolated from WT and *msl1-1* seedlings. After labelling with the membrane-potential-independent dye MitoTracker Green (MTG), mitochondria were subjected to hypo-osmotic shock and were visualized under CLSM (Figure 3B). Mitochondrial volumes were calculated from Z-stacks (Figure 3C) and it is apparent that as the concentration of osmoticum decreases, the mitochondria swell. However, the degree of swelling was not significantly different between WT and *msl1-1*. When osmoticum was completely omitted,

the majority of mitochondria appeared ruptured, but the number of intact mitochondria that remained was the same in *msl1-1* and WT mitochondria. These data demonstrate that MSL1 does not provide substantial protection against rupture from hypo-osmotic shock in isolated mitochondria.

Loss of MSL1 leads to increased membrane potential in isolated mitochondria when F_1F_0ATPsynthase is inactive

Given that MSL1 is essentially non-selective with respect to ion species (Figure 2D) and that these channels are not known to exclude H^+ or K^+ (Naismith and Booth, 2012; Maksaev and Haswell, 2012; Cox et al., 2013; Hamilton et al., 2015b) opening of MSL1 would be expected to lead to partial dissipation of the mitochondrial membrane potential ($\Delta\Psi_M$). We therefore sought to determine the effect of MSL1 on $\Delta\Psi_M$ of isolated mitochondria and to use this readout to explore the conditions under which MSL1 is active. Isolated mitochondria from WT and *msl1-1* and the complemented line, *msl1-1/gMSL1,* were energized with respiratory substrates and labelled with MTG and the cationic lipophilic fluorescent molecule tetramethyl rhodamine methyl ester (TMRM). The use of these two fluorescent probes provides a ratiometric estimation of membrane potential given that accumulation of TMRM in mitochondria is $\Delta\Psi_M$-dependent, while MTG accumulates in a $\Delta\Psi_M$-independent manner, providing a reference control. TMRM and MTG fluorescence were quantified by CLSM imaging (Figure 4A). When mitochondria were energised with succinate, a significantly higher proportion of *msl1-1* mitochondria had a higher TMRM:MTG fluorescence ratio than WT and the complemented line (Figure 4B), demonstrating that loss of MSL1 leads to higher $\Delta\Psi_M$ in the presence of respiratory substrate but no ADP. Similar results were obtained when malate and pyruvate were used as respiratory substrates (Figure 4C), suggesting that under state II conditions when the F_1F_0 ATP synthase is inactive due to lack of ADP and the $\Delta\Psi_M$ is thus high, the MSL1 channel is active in WT and complemented lines. This would serve to limit the maximum membrane potential that can be reached.

To establish whether the bioenergetic state of the mitochondrion influences MSL1 function, we repeated the analysis with mitochondria in state III (supplied with succinate and ADP). As expected, the activation of the F_1F_0 ATP synthase caused a decrease in $\Delta\Psi_M$ measured as a decrease in the TMRM:MTG fluorescence ratio. Additionally, it was apparent that there was no longer a difference in TMRM:MTG ratio between the genotypes (Figure 4D). To confirm that the genotype response under state III conditions was due to ATP synthase activity,

oligomycin was added to inhibit ATP synthase and this restored the difference in TMRM:MTG ratio between genotypes (Figure 4E). Hence, loss of MSL1 leads to an increased $\Delta\Psi_M$ compared to WT, but only under state II conditions when F_1F_0 ATP synthase is inactive. Given that opening of a non-selective ion channel such as MSL1 would dissipate $\Delta\Psi_M$, this is likely a direct consequence of the absence of MSL1, although an indirect or secondary effect cannot be ruled out.

MSL1 is not responsible for $\Delta\Psi_M$ pulsing, but loss of MSL1 creates conditions that increase pulsing

Some of the frequency distribution histograms of the TMRM:MTG fluorescence ratio in individual isolated mitochondria taken at single time-points (Fig. 4) appear bimodal. One possible cause of bimodal populations of $\Delta\Psi_M$ is membrane potential pulsing which is prevalent in isolated mitochondria in state II (Schwarzländer et al., 2012). These $\Delta\Psi_M$ pulses are frequent in state II (on a time scale of seconds to minutes) and rather irregular in frequency and amplitude (Schwarzländer et al., 2012). Hence in a snapshot of a population of mitochondria (as shown in Fig. 4), some mitochondria will be between pulses (higher $\Delta\Psi_M$) and some will be in a pulse (lower $\Delta\Psi_M$), leading to two peaks in the TMRM:MTG frequency distribution histograms. Moreover, the state II bioenergetic condition that promotes pulsing is the same condition under which loss of MSL1 affects $\Delta\Psi_M$, raising the possibility that transient opening of MSL1 could be responsible for pulsing. To investigate this further, we quantified $\Delta\Psi_M$ (from TMRM fluorescence) over a timecourse in multiple individual isolated state II mitochondria from WT and *msl1-1* and the complemented line (Figure 5). As expected, State II WT mitochondria showed frequent $\Delta\Psi_M$ pulses (Figure 5A). However, frequent $\Delta\Psi_M$ pulsing was also apparent in state II *msl1-1* mitochondria meaning that MSL1 is not the channel responsible for pulsing. Frequency distribution histograms of the complete set of these timecourse data were plotted for populations of mitochondria from WT, the *msl1-1* knockout and the complemented line (Figure 5B) and, as in the single time point snapshots of Figure 4, a bimodal distribution was apparent that could be fitted with a two-component Gaussian mixture model. The same analysis was done for mitochondria from the three genotypes under state III (in the presence of ADP). As expected this dramatically reduced the extent of pulsing in all genotypes (Figure 5C) and decreased $\Delta\Psi_M$ (Figure 5D). We previously established that the best statistical measure of the amount of pulsing is given by the coefficient of variation (CV) of $\Delta\Psi_M$ over time for each mitochondrion (Schwarzlander et al., 2012). The mean CV from multiple mitochondria revealed that the

amount of pulsing was significantly greater in the *msl1-1* mutant (Figure 5E). Additionally, the proportion of the population of mitochondria that was pulsing (given by the area under the left-hand peak in the TMRM:MTG frequency distribution histogram with decreased $\Delta\Psi_M$) was also significantly greater in the *msl1-1* mutant (Figure 5G), suggesting a greater frequency or duration of pulsing. Finally, to provide a robust measure of the resting $\Delta\Psi_M$ (i.e. between pulses) and to confirm the apparent increase in $\Delta\Psi_M$ in the *msl1-1* line in state II mitochondria shown in Figure 4, we determined the mean TMRM:MTG value of the right-hand peak of the frequency distribution corresponding to the higher $\Delta\Psi_M$ that occurs between pulses. This confirmed a significant increase in $\Delta\Psi_M$ in the *msl1-1* mutant in comparison to the WT and complemented line (Figure 5G) consistent with the data from single time-points (Figure 4). In summary, we infer that MSL1 is not directly responsible for $\Delta\Psi_M$ pulsing but that loss of MSL1 does increase pulsing frequency and amplitude. The most likely role of MSL1 is thus to help to limit build-up of excessive membrane potential during temporary bioenergetic imbalance. Likewise, loss of MSL1 may exacerbate, the bioenergetic conditions that cause pulsing (high membrane potential and ROS production).

The effect of MSL1 on $\Delta\Psi_M$ in isolated mitochondria is moderated by ROS scavengers and antioxidants.

When mitochondria are energised by respiratory substrate but ATP synthase is not active (state II), the respiratory chain becomes highly-reduced and the rate of mitochondrial ROS production increases (Møller, 2001). This phenomenon and the changes in pulsing (Figure 5) raise the possibility that MSL1 channel function is influenced by the redox status of mitochondria. To test this, we incubated state II mitochondria with a range of different antioxidants, free radical scavengers and lipid peroxidation inhibitors (Figure 6). If MSL1 is directly activated by the ROS produced in state II mitochondria, then we would expect the addition of ROS scavengers to increase WT membrane potential to mutant values, i.e. the prevention of ROS-activation of MSL1 under state II conditions, would mean that it no longer serves to dissipate $\Delta\Psi_M$. Thus, by preventing activation of MSL1 by ROS, the WT could be expected to phenocopy the knockout mutant. This behaviour is what was observed when the matrix-accumulating antioxidant MitoTEMPOL was added. However, a less clear picture emerged when other ROS-ameliorating agents were used. For example, addition of MitoQ which specifically prevents inner membrane lipid peroxidation (Kelso et al., 2001; Murphy and Smith, 2007), abolished the difference in $\Delta\Psi_M$ between *msl1-1* and WT, but not by increasing WT $\Delta\Psi_M$ to the level expected in the *msl1-1* mutant, but by reducing $\Delta\Psi_M$ in the *msl1-1* mutant to WT levels. This was not the result of a non-specific uncoupling effect of

MitoQ because the control analogue decyl triphenylphosphonium (dTPP) which lacks antioxidant activity did not alter $\Delta\Psi_M$ in the *msl1-1* mutant. The antioxidant, ascorbate, also had a similar effect to MitoQ whereas the matrix-accumulating superoxide dismutase mimetic MnTMPyP had no effect. These data suggest that alterations in mitochondrial ROS can affect MSL1 activation state but there is also evidence that loss of MSL1 alters the sensitivity of mitochondria to the antioxidants MitoQ and ascorbate. The interaction between MSL1, ROS and $\Delta\Psi_M$ is complex, and appears to depend on the local origin and type of ROS produced. At this stage we do not have a clear understanding of the mechanism behind these interacting indirect effects.

MSL1 is crucial for regulating mitochondrial redox status during abiotic stress

So far we have demonstrated that the presence of MSL1 is important under bioenergetic conditions in which the respiratory chain is likely to become highly reduced and the rate of mitochondrial ROS production would increase. This bioenergetic state can often be triggered by abiotic stresses due to disruption of normal electron transport or general alterations in redox and energy balance (Møller, 2001). To establish whether MSL1 is important during abiotic stress we monitored the *in vivo* mitochondrial redox status of WT and *msl1-1* roots expressing a mitochondria-targeted roGFP2 that reports on the redox poise of the mitochondrial glutathione pool (mito-roGFP2) (Schwarzländer et al., 2015) subjected to various pharmacological treatments and stresses (Figure 7). Figure 7A shows false-coloured images of the ratio of mito-roGFP2 fluorescence collected with 405 and 488nm excitation wavelengths. An increase in this ratio corresponds to greater oxidation of the roGFP2 probe and indicates greater oxidation state of the glutathione pool in the mitochondrial matrix (Schwarzländer et al., 2015). As expected, incubation of roots with oligomycin to inhibit mitochondrial ATP synthase increased the oxidation of mito-roGFP2 in WT mitochondria (Figure 7A, B), because the reduced ATP synthase activity leads to over-reduction of respiratory chain complexes and subsequent ROS production in the mitochondrial inner membrane. The increase in roGFP2 oxidation in response to oligomycin treatment was substantially greater in the *msl1-1* mutant than in WT, demonstrating that loss of MSL1 compromises the ability of mitochondria to maintain redox homeostasis *in vivo*. The involvement of mitochondrial bioenergetic imbalance was confirmed by the addition of a membrane uncoupler, carbonyl cyanide m-chlorophenyl hydrazone (CCCP) which restored mito-roGFP2 oxidation state to WT values (Figure 7B). The involvement of ROS was confirmed by the restoration of *msl1-1* mito-roGFP2 oxidation state to WT values by the addition of ascorbate (Figure 7B). Addition of antimycin A, which is known to raise

mitochondrial membrane potential and generate mitochondrial ROS by inhibition of the Q cycle in complex III (Quinlan et al., 2011) also caused an increase of mito-roGFP2 oxidation state in *msl1-1*, but rotenone, an inhibitor of complex I, had no effect (Figure 7B). In contrast, addition of propranolol, which prevents the uptake of inorganic anions as well as di- and tricarboxylates by the plant inner mitochondrial membrane anion channel (PIMAC; Beavis, 1992; Laus et al., 2008), reduced the roGFP2 oxidation state to a similar degree in WT and *msl1-1*.

We also examined the mito-roGFP2 oxidation state in roots exposed to a range of stress conditions, namely salt-, osmotic-, heavy- metal- and high-temperature-stress (Figure 7C). As found previously (Schwarzländer et al., 2012), salt stress did not affect the oxidation of a mitochondria-targeted roGFP2 in WT roots and there was no significant difference between WT and *msl1-1*. Similarly, there was no effect of absence of MSL1 on mito-roGFP2 following hyper-osmotic stress (150 mM and 300 mM mannitol treatments), with both a slight decrease in mito-roGFP2 oxidation in both WT and *msl1-1* roots. This corroborates the osmotic-shock assays on isolated mitochondria (Figure 3). In contrast, high temperature (44^{o}C for 10 min) caused a significant increase in mito-roGFP2 oxidation in WT roots (Figure 7C) and this was significantly exacerbated in *msl1-1* roots. At a more extreme temperature (48^{o}C for 5 min) roGFP2 became more oxidised (around 60% oxidised) and the difference between *msl1-1* and WT disappeared (Figure 7C). There was also a significant increase in mito-roGFP2 oxidation in *msl1-1* compared to WT roots treated with 3 or 5 mM Cd^{2+}. Collectively, these data demonstrate that loss of MSL1 exacerbates mitochondrial glutathione pool oxidation under specific abiotic stresses and suggest that MSL1 may provide a mechanism for maintenance of mitochondrial redox status under stress.

DISCUSSION

Our data demonstrate that MSL1 is a stretch-activated non-selective ion channel (Figure 2). Stretch activation provides a regulatory mechanism that allows the channel to respond to cell / organellar swelling due to hypo-osmotic stress. The resultant release of ions reduces osmotic potential and can protect against hypo-osmotic shock, which is thought to be an important function of MscS homologues in *E. coli* and in Arabidopsis plastids and pollen grains. And although *E. coli* expressing MSL1 show enhanced tolerance of hypo-osmotic shock, we did not find strong evidence that MSL1 fulfils this role in Arabidopsis mitochondria (Figure 3). In isolated mitochondria, reduction of the osmotic potential of the incubating medium had only a minor effect on WT mitochondrial volume indicating a robust mechanism

for volume homeostasis. Absence of MSL1 had no significant effect on this response because the osmotic shock we administered was too severe or too rapid for MSL1 to have an effect, or possibly due to redundant osmoregulatory mechanisms, as in *E. coli* (Levina et al., 1999). In chloroplasts, osmotic pressure and ion homeostasis are controlled not only by MSL2 and MSL3 (Valey et al., 2012), but also by a family of K^+/H^+ antiporters (KEA) that work cooperatively with other cation channels (Kunz et al., 2014). A similar K^+/H^+ antiporter (KHE) also exists in plant mitochondria, although its molecular identity remains unknown to date (Hensley and Hanson, 1975; Diolez and Moreau, 1985; Trono et al., 2015). Nevertheless, it is also notable that treatment of WT and *msl1-1* roots with hyper-osmotic concentrations of mannitol did not cause a significant increase in oxidation of the mitochondrial glutathione pool (Figure 7C), suggesting that MSL1 is not a major part of the mechanism that maintains mitochondrial redox poise under this stress condition. Instead, our data point to MSL1 being important under conditions of bioenergetic imbalance characterised by high $\Delta\Psi_M$ and a potential high-reduction state of the respiratory chain leading to ROS production (Figure 4 and 5). The increased impact of high temperature and Cd^{2+} treatments on the oxidation state of mitochondrially-targeted roGFP2 in roots of *msl1-1* knockout mutants (Figure 7C) demonstrates that MSL1 is an important component of the molecular machinery that maintains mitochondrial redox status under these specific stresses. Both of these stresses are known to cause bioenergetic imbalances in mitochondria (Lin and Markhart, 1990; Kesseler and Brand, 1994b, a, c; Atkin et al., 2002) and also stimulate mitochondrial pulsing (Schwarzlander et al., 2012). Indeed, in isolated mitochondria, MSL1 functions in the same bioenergetic conditions that lead to pronounced pulsing, whilst a lack of MSL1 enhances the extent of pulsing, suggesting that the two mechanisms are complementary. Given that opening of MSL1 would cause dissipation of $\Delta\Psi_M$ it is likely that, similar to pulsing, MSL1 acts as a release valve to avoid over-reduction of the respiratory chain and ROS production due to the build-up of a very high $\Delta\Psi_M$.

Clearly, an important feature of such an uncoupling ion channel would be that it selectively opens only when the mitochondria are in this unbalanced bioenergetic state. One possibility is that the channel is gated or modulated by high negative transmembrane voltage. Although we saw some evidence of this in patched-clamped *E. coli* spheroplasts expressing MSL1, the instability of spheroplast membranes at high negative voltages made it impossible to characterise this behaviour in more detail. An alternative possibility is that high $\Delta\Psi_M$ leads to changes in membrane tension and this leads to activation of MSL1. This could be mediated by damage to membrane lipids by ROS, leading to altered conformation and tension of the membrane. A final possibility is that the MSL1 channel could be directly activated by ROS

via oxidation of amino acid side groups in such a way that alters the membrane tension threshold for channel opening (Ridone et al., 2015). We explored the effect of reducing ROS *in vivo* using mitochondrially-targeted antioxidants (Figure 6). In one case (MitoTEMPOL), we found effects consistent with ROS activation of MSL1 in that MitoTEMPOL increased $\Delta\Psi_M$ in WT mitochondria to levels observed in the *msl1-1* mutant. Other antioxidants also abolished the differences in state II mitochondrial membrane potential between WT and the *msl1-1* mutant, but via unexplained indirect effects that operated in the *msl1-1* mutant background rather than in WT plants with functional MSL1. These differences could be related to the different mode of action of the antioxidant reagents used. MitoTEMPOL consists of an antioxidant piperidine nitroxide group conjugated to the lipophilic cation trimethylphosphonium that delivers the nitroxide group to the matrix face of the inner membrane in a membrane-potential-dependent fashion (Murphy and Smith, 2007). The nitroxide group can catalyse the dismutation of superoxide and detoxify Fe^{2+} ions (Samuni et al., 1990; Bar-On et al., 1999; Trnka et al., 2009) thereby preventing Fenton chemistry that leads to hydroxyl radical formation. In contrast, MitoQ delivers the antioxidant ubiquinone into the hydrophobic core of the inner membrane preventing lipid peroxidation (Murphy and Smith, 2007), while ascorbate detoxifies hydrogen peroxide via matrix-localised ascorbate peroxidase activity. The contrasting effects of these antioxidants may suggest that a direct oxidation of the MSL1 protein by hydroxyl radicals may be a potential activating mechanism rather than alteration of membrane tension via lipid peroxidation, but more detailed studies would be required to establish this.

Our characterization of MSL1 means that it now sits alongside a growing cast of players that act to uncouple plant mitochondria. These include mitochondrial membrane potential pulsing (Schwarzländer et al., 2012), UCP (Vercesi et al., 2006), and alternative respiratory pathways generated by electron flow via the alternative NAD(P)H dehydrogenases (Rasmusson et al., 2004) and alternative oxidase (Moore et al., 2013). Moreover, it is clear that MSL1, pulsing and UCP all respond in various ways to mitochondrial ROS and / or mitochondrial membrane lipid peroxidation. The effect of activation of these three ion transport processes is the same – to dissipate $\Delta\Psi_M$ – leading to the question of why more than one mechanism is necessary to achieve the same end. We show here that other uncoupling processes cannot completely compensate for a loss of MSL1: the mitochondrial glutathione pool (as indicated by the degree of mito-roGFP2 oxidation) is more oxidised in the *msl1-1* mutant under specific abiotic stress conditions and when the mitochondrial bioenergetic state is directly manipulated with respiratory inhibitors (Figure 7B). This is

despite the observation that loss of MSL1 causes an increase in pulsing (Figure 5). This suggests that MSL1, pulsing and UCP are non-redundant *in planta*.

Three reasons can be envisaged for multiple routes to mitochondrial uncoupling. Firstly, it is possible that different mechanisms could lead to activation at different levels of mitochondrial respiratory chain over-reduction. The second reason could be related to capacity in different cell types. The abundance of the transporters and channels responsible could be quite different leading to different capacities for uncoupling. Combined with different activation thresholds, this would allow a fine tuning of the response, which may be important to dampen bioenergetic imbalance while minimising the effect on ATP synthesis. Finally, it is evident that the different uncoupling mechanisms operate on different timescales and this could be important in allowing both short- and long-term homeostasis and adaptation to environment. In particular, the alternative respiratory pathways appear to be largely regulated at the transcriptional level (Escobar et al., 2004; Clifton et al., 2005), which means they allow relatively long-term adjustments to environmental stress. In contrast, pulsing operates on the timescale of less than one minute (Schwarzländer et al., 2012) and MSL1 function is also likely to be rapid given the timescale of its response to bioenergetic state changes in isolated mitochondria. It is possible that MSL1 may function to limit increases in mitochondrial membrane potential prior to the onset of pulsing.

In summary, we have shown that MSL1 is a stretch-activated ion channel with electrophysiological similarities to its homologues from *E. coli* and Arabidopsis. While mitochondrially-localised MSL1 can confer protection from osmotic shock onto *E. coli* lacking key bacterial mechanosensitive channels, it does not protect isolated mitochondria against lysis under hypo-osmotic shock. Instead, we demonstrate that MSL1 function is apparent when mitochondrial membrane potential is high, which is also a condition that leads to mitochondrial ROS production and lipid peroxidation. We also show that the absence of MSL1 loads a greater oxidative burden on mitochondria under abiotic stress, reflected in an increased oxidation of the mitochondrial glutathione pool.

METHODS

Plant Materials and Growth Conditions

Arabidopsis thaliana (ecotype Columbia-*0*) seedlings and plants were grown under a light intensity of 50 µmol $m^{-2}s^{-1}$ with a photoperiod of 16 h after seeds were stratified at 4°C in the dark for 2-3 days. The *msl1-1* T-DNA insertion line was obtained directly from GABI-Kat (GK-844G07). Plants were grown on compost supplemented with Vermiculite. For the isolation of mitochondria, seeds were surface-sterilized and grown in Murashige and Skoog (MS) medium (½-strength MS medium, 2 mM MES pH 5.7) supplemented with 1% (w/v) sucrose and 0.1% (w/v) agar for 14-16 days with gentle agitation (40-60 rpm). For growth assays or *in vivo* confocal laser scanning microscopy (CLSM) of roots, seedlings were grown for 5-6 days on vertical plates containing ½-MS medium and 1.5% (w/v) agar.

Generation of MSL1 transgenic lines and mutant identification

Plants homozygous for a T-DNA insertion in the first exon of *MSL1* were identified by PCR of genomic DNA using the following primer pairs: MSL1_F and MSL1_R; T-DNA_F and T-DNA_R (Supplementary Table 1). To visually confirm the absence of *MSL1* transcript in the insertion line, cDNA was synthesized from DNase-treated total RNA as previously described (Birke et al., 2013) and semi-quantitative PCR was carried out with the primer pair MSL1_sqPCR_F and MSL1_sqPCR_R (Supplementary Table 1). Quantitative RT-PCR was performed in a Rotor-Gene Q cycler (Qiagen) using the Rotor-Gene SYBR Green PCR kit (Qiagen) according to the manufacturer's instructions with the primers MSL1_qPCR_F and MSL1_qPCR_R (Supplementary Table 1). The amount of MSL1 protein in the transgenic lines was quantified by immunoblotting using a peptide antibody raised against the C-terminus of the MSL1 protein (see below).

The *MSL1* genomic complementation transgene *MSL1g* was made by amplifying the entire *MSL1* genomic region, including the promoter, 5', and 3' UTRs from wild-type Columbia DNA with oligos LHO710 and LHO817 (Supplementary Table 1). The resulting 3.6 kb fragment was cloned via the Gateway system into pENTR/D-TOPO and then into the destination binary vector pBGW. The complemented lines were generated by agrobacteria-mediated transformation of the pBGW-MSL1g construct. Primary transformants were screened for BASTA resistance and the presence of *MSL1* transcript by RT-PCR. After two generations (T_2), a segregation analysis was performed and the homozygous complemented line with approximately equal amount of *MSL1* transcript as Col-0 was chosen for further analysis.

For generating the MSL1-GFP construct, the *MSL1* open reading frame was amplified from leaf cDNA with MSL1-GFP_F and MSL1-GFP_R (Supplementary Table 1) and cloned via the Gateway system into pENTR/D-TOPO and then into the destination binary vector pK7FWG2. This construct was then introduced into Col-0 by Agrobacterium-mediated transformation. To generate the *msl1-1*/roGFP2 line, the homozygous *msl1-1* line was crossed with a transgenic line carrying a roGFP2 construct (Schwarzländer et al., 2008).

Isolation and fractionation of mitochondria

Mitochondria were isolated from two-week-old Arabidopsis seedlings as described previously (Sweetlove et al., 2007). Fractionation of mitochondria into peripheral and integral membrane fractions was carried out according to Millar et al. (2001) with slight modifications. Briefly, 1 mg of mitochondrial proteins was resuspended in 100 µl of 20 mM TES (2-[(2-Hydroxy-1,1-bis(hydroxymethyl)ethyl)amino]ethanesulfonic acid) buffer (pH 7.5) and incubated for 10 min. Following three freeze-thaw cycles, the pellet containing membrane-associated proteins was collected by centrifugation at 20,000 x g for 25 min. It was then resuspended in 100 µl of 100 mM Na_2CO_3 (pH 11.5) and incubated on ice for 20 min. The resulting sample was centrifuged at 20,000 x g to collect the peripheral and integral membrane fractions in the supernatant and pellet respectively. The pellet was resuspended in blue-native solubilisation buffer containing digitonin before loading onto a blue native- or SDS-PAGE.

Mitoplasts were obtained by hypo-osmotic shock of mitochondria, using a method described previously (Murcha et al., 2003). To determine the topology of proteins, 750 µg of mitochondria or mitoplasts were treated with 24 µg/ml proteinase K (Sigma-Aldrich) or water on ice. Following 30 min incubation, 1 mM PMSF was added to the samples to stop the reaction. Mitochondria or mitoplasts were collected by sedimentation at 20,000 x g for 20 min. This step effectively removed unpelleted proteins in the intermembrane space in the mitoplast fraction. The pellet was resuspended in 75 µl of 100 mM Na_2CO_3 (pH 11.5) and integral membrane proteins were extracted as described above. *In vitro* import of MSL1 into isolated mitochondria and chloroplasts was carried as described previously (Duncan et al., 2015).

CLSM and data analysis

Freshly isolated mitochondria (in 1 mg/ml) were incubated in 500 nM MitoTracker Green in minimum medium (0.3 M sucrose, 10 mM TES and pH 7.2 (adjusted with NaOH)) for 30 min at 4°C. Mitochondria were then immobilized onto round glass cover slides by centrifugation in minimum medium at 2,000 x g for 5 min at 4°C with brake off. Immobilized mitochondria were energized by the addition of a minimum medium containing respiratory substrates and/or effectors (as stated in the text and in figure legends) and labelled with 25 nM TMRM for state II respiration or 100 nM TMRM for state III respiration. Microscopy was performed using a Zeiss LSM510 META confocal microscope (Carl Zeiss MicroImaging) equipped with laser lines for 488-and 543-nm excitation. Images were collected with a 60× lens (Zeiss 60× 1.4 N.A. Plan-Apochromat oil-immersion lens) for in multi-track mode with line switching between channels. Excitation/emission wavelengths were selected for different probes as follows: TMRM, 543/565-615 nm and MitoTracker Green, 488 nm/505-530 nm. The pinhole diameter was 1.2-1.4 airy units depending on the emission band-pass filter, but the optical slice was kept constant at 1.0 µm for all channels. All other imaging parameters, including laser power of both excitation channels, were kept constant throughout all measurements. CLSM z-stack (10x 0.2 µm) and time series data (3 s interval in the total of 2-3 min) of mitochondria were analysed using a custom Matlab program available from www.markfricker.org (Fricker, 2015). In brief, the mitochondria were automatically separated into unique domains using a watershed algorithm and individually segmented with a local intensity threshold set at the mid-point between each object and the background. This was required to ensure that objects with different intensity values were segmented correctly, which was not possible with a single, global intensity threshold. The average fluorescence intensity at each wavelength were measured for each mitochondrion, and the volume estimated from the projected area assuming spherical geometry.

CLSM imaging of MSL1-GFP seedlings was performed using a FLUOVIEW FV1000 (Olympus) and images were captured with FVIO-ASW software (Olympus). GFP signal was excited at 488 nm and emissions collected with a 505-520 nm bandpass filter. Mitotracker was excited at 543 nm and emissions collected with 560-620 BP filter. Chlorophyll autofluorescence was excited at 635 nm and emissions collected with a 655-755 nm BP filter.

For ratiometric in vivo imaging of 5-6 day old roGFP2-expressing seedlings, a Nikon A1Si confocal microscope equipped with laser lines 405- and 488-nm excitation and emission band-pass filter of 500-520 nm and controlled by a NIS-Elements AR software package (version 4.13.01, Build 916) was used. Images were acquired in the '2Ex 1Em' mode using a 20x lens (Nikon CFI Plan Apo VC 20X 0.75 N.A.) with pinhole diameter of 2.5 airy units (corresponds to the optical slice of 4.37 µm). The 405/488-nm laser power ratio of 6:1 for imaging roGFP2 was kept constant for all treatments as indicated. The 405/488-nm fluorescence ratios and the degree of oxidation of roGFP2 were calculated using the same custom Matlab program described above (available from www.markfricker.org; Fricker, 2015). In brief, this approach finds the brightest voxel in z with excitation at 488nm, and then collects the equivalent voxel from the 405 and autofluorescence channels before background subtraction and ratioing (Fricker, 2015). Calibration of the roGFP2 probe was carried out using 10 mM DTT (full reduction) and 10 mM H_2O_2 (full oxidation) and the degree of oxidation of roGFP2 was calculated according to Schwarzländer et al. (2008).

Molecular cloning and expression of MSL1

The gene corresponding to the mature version of MSL1 (i.e. without the first 79 amino acid residues that constitute the mitochondrial targeting sequence) was amplified with the primer pair His-MSL1-m_F and His-MSL1-m_R (Supplementary Table 1). The PCR product was then subcloned into an entry vector using a pENTR/D-TOPO cloning kit. MSL1 was then cloned into a Champion pET300/NT-DEST vector (Life Technologies) by Gateway LR reaction, and the resulting construct was transformed into *Escherichia coli* Rosetta strain. Before induction, bacteria were inoculated in 40 ml LB medium containing 1% glucose, 200 µg/ml Ampicillin and 34 µg/ml chlorophenicol. Following overnight pre-induction, cells were collected by centrifugation (4,000 x g for 15 min), and the resulting pellet was resuspended in fresh LB-medium. Bacteria were added to 200 ml LB-medium containing 1% glucose and antibiotics to achieve the final OD_{550nm} of at least 0.4. Induction was carried out overnight at 28°C after the addition of 1 mM IPTG. Cells were harvested by centrifugation (4,000 x g for 20 min) and the pellet was resuspended and clarified in 10 ml lysis buffer (50 mM phosphate buffer pH 8.0, 300 mM NaCl and 10 mM imidazole) containing 0.5% (v/v) Triton X-100. Following centrifugation to remove insoluble materials (e.g. inclusion bodies), proteins in the supernatant was separated overnight by a 4.5-16% BN-PAGE and the identity of the MSL1 band was confirmed by immunoblotting and mass spectrometry (see below).

Inserts for pCTC-His6-MSL1 and pCTC-MSL1-FLAG were amplified from pET300-MSL1 using LHO2458 and LHO2459 or LHO2460 and LHO2462, respectively (Supplementary Table 1). PCR products were inserted into pCTC-FLAG (Sigma) digested with EcoRI and SalI using a Gibson Assembly Cloning Kit (NEB).

Polyacrylamide gel electrophoresis, immunoblotting and mass spectrometry

To produce a specific antibody against AtMSL1, a homology modelling was performed, using the known structure of *E. coli* MscS (Bass et al, 2002; Steinbacher et al., 2007) as a template, to determine the peptide sequence where it is exposed to the aqueous environment that allows recognition and binding by the epitopes. Antibodies against the peptide sequence QISNEIKEMLRSNTK were produced in rabbits (Eurogentec Inc.). Purified antibodies were used in 1:1000 for probing the native form of MSL1.

Separation of digitonin-solubilized mitochondrial proteins was carried out according to Eubel et al. (2003) using a 4.5%-16% gradient BN gel dimension and a two-step Tricine-SDS second dimension (8% and 12%). For western blotting, BN gels and PVDF membranes were equilibrated in a modified transfer buffer (48 mM tris, 15 mM bis-tris and 2.5 mM tricine at 4°C). Protein transfer was carried out using a semi-dry FastBlot B43 system (Biometra) at 0.5 mA per square centimetre of gel for 3 h at 4°C.

For Western blotting with 1D SDS-PAGE, 20 µg proteins were separated by SDS-PAGE using a Hoefer MiniEV systems and transferred to PVDF or nitrocellulose membranes for immunodetection by standard procedures using horseradish peroxidase-conjugated secondary antibody. Transferred proteins were probed with primary antibodies specifically targeted to MSL1 (1:1000), Porin (1:5000; (Lee et al., 2008)), SLP2 (1:5000, (Gehl et al., 2014)), cytochrome c (1:1000; Balk et al., 1999), and penta-His (Anti-His Antibody Selector Kit, Qiagen).

For protein identification, gel pieces were destained in 25 mM ammonium bicarbonate in 50% acetonitrile, reduced (10 mM DTT, 37 ºC, 30 minutes) and alkylated (55 mM iodoacetamide, 25 ºC, one hour). Trypsin digest (200 ng (Promega) in 25 mM ammonium bicarbonate) was performed at 37 ºC overnight. Extracted peptides were concentrated in a SpeedVac (ThermoSavant). Samples were then processed for protein identification at the Central Proteomics Facility, Dunn School of Pathology, University of Oxford. Briefly, samples

were resolved on a 25 cm by 75 µm diameter column in an Ultimate 3000 nanoRSLC system (Dionex) at 300 nl/min flow rate using a 125 minute gradient before detection in a Q Exactive mass spectrometer (Thermo). Sample Data were queried using Mascot Search Engine (version 2.4, MatrixScience, London) against UniProtCP_arath. Search criteria were trypsin with two missed cleavage sites allowed; fixed modification was carbamidomethyl (C), variable modification was oxidised (M). Precursor mass tolerance was +/- 20 ppm and fragment mass tolerance was +/- 0.02 Da.

Osmotic Shock Assays

Bacterial osmotic downshock assays were performed essentially as described in Bartlett et al. (2004). Cultures of bacteria (transformed either with a pCTC-FLAG, pCTC-His6-MSL1 or pCTC-MSL1-FLAG construct) were inoculated from newly transformed colonies and grown overnight at 37°C, then diluted 1:10 and grown until an OD_{600} of 0.1. IPTG induction was for 2 hours.

Electrophysiology

Giant spheroplasts were made essentially as described in Martinac et al. (2013), with the following modifications. *E. coli* cell cultures were treated with cephalexin for 1.5 hour and then induced with 1 mM IPTG for 2 hours. Spheroplasting was carried out at room temperature for 20 min. The resulting suspension was centrifuged through 7 mls of 1 M sucrose, resuspended in 1 M sucrose, and stored in aliquots at -20°C or -80°C.

Patch-clamp experiments were performed using a pipette buffer (200 mM KCl, 90 mM $MgCl_2$, 5 mM $CaCl_2$, 5 mM Hepes, pH 7.4) and a bath buffer (same as pipette with added 400 mM sucrose). Excised inside-out patches (using pipettes with bubble number ~4.5 (Schnorf et al. (1994)) from spheroplast membranes were treated with 5-second triangle pressure ramps of amplitudes from -40 mmHg to -200 mmHg. Data were collected using Axopatch 200B amplifier and Digidata 1440 digitizer (Molecular Devices) at 20 kHz and filtered at 5kHz. Data were analyzed with Clampfit 10.5 (pCLAMP 10 software suite, Molecular Devices).

The ion selectivity of MSL1 was probed under asymmetric buffer conditions. Inside-out patches were excised in symmetric buffer (200 mM KCl, 90 mM $MgCl_2$, 5 mM $CaCl_2$, 5 mM Hepes, pH 7.3). Then the bath was perfused with a high salt solution (600mM KCl, 90mM $MgCl_2$, 5mM $CaCl_2$, 5mM Hepes, pH 7.3). The value of reversal potential was calculated as

the point of intersection of voltage axis with a line representing a linear fit of unitary current in the range between 40 mV and -50 mV membrane potential.

Acknowledgements

CPL was supported by a European Molecular Biology Organization (EMBO) long-term fellowship (ALTF 1140-2011). CPL also acknowledges support from the CellNetworks Excellence Cluster Postdoctoral Program (University of Heidelberg) to initiate this work.

AHM was support by the ARC (Australian Research Council) Centre of Excellence in Plant Energy Biology [grant numbers CE140100008; FT110100242]

ESH acknowledges the support of the NIH (National Institutes of Health) grant number 2R01GM084211-5A1.

We also acknowledge the Centre for Microscopy, Characterisation & Analysis (CMCA) at the University of Western Australia for the use of facilities and technical assistance.

Finally, we would like to thank Mike Murphy (Medical Research Council Mitochondrial Unit, Cambridge, UK) for providing MitoQ.

Supplementary Figure 1. The MSL1 precursor is not imported into isolated chloroplasts *in vitro*. Radiolabelled MSL1 precursor was incubated with purified chloroplasts under conditions that support protein uptake (first panel). Following import, thermolysin treatment was conducted as indicated. The uptake of small subunit of RUBISCO (SSU) was used as a positive control for chloroplast import (second panel). p, precursor protein; m, processed mature protein.

Supplementary Figure 2. Characterization of *msl1-1*-knockout and complemented lines of Arabidopsis. (A) Schematic showing location of the T-DNA insertion in the *MSL1* gene. (B) Semi-quantitative RT-PCR showing loss of transcript in *msl1-1* and its restoration in the complemented line. (C) The loss and restoration of MSL1 protein in the mutant (*msl1-1*) and complemented line (*msl1-1*/gMSL1) is demonstrated by western blot of peripheral and membrane fractions of mitochondria using antibody against MSL1 (also refer to Figure 1C for a more detailed figure legend). (D) Phenotype of *msl1-1*-knockout and complemented lines grown on agar plates and soil.

Supplementary Figure 3. Verification of MSL1 expression in *E. coli*. (A) SDS-PAGE of Triton X-100-soluble (lane A, total cytoplasmic and membrane fraction) and –insoluble (lane B, fraction of inclusion bodies) proteins following overexpression of MSL1 in *E. coli*. Proteins

were either visualized directly by Coomassie blue staining (left) or transferred onto a PVDF membrane for immunoblotting with an antibody against penta-histidine tag (right). The location of MSL1 band on the gel is indicated by a black triangle. (B) 1D Blue Native/SDS-PAGE of Triton X-100-solubilized fraction from *E. coli* expressing either RAC-kinase (lane 1, control) or mature MSL1 (lane 2). Proteins were either visualized directly by Coomassie blue staining (left) or transferred onto a PVDF membrane for immunoblotting with a peptide antibody raised against MSL1 (right). The location of MSL1 band on the Coomassie-stained gel is indicated by a black triangle.

Supplementary Figure 4. Comparison of tension-gated MSL1 channel activity under positive and negative membrane potentials.

Supplementary Data 1. Identification of MSL1 by Mass spectrometry. Excel file includes a list of peptides detected in this study and in published literature. Three MGF files contain the identity of all peptides/proteins in the MSL1-containing protein spot extracted from three independent fractionation of isolated mitochondria on Blue-Native/SDS-PAGE.

Supplementary Table 1. A list of primers used in this study.

REFERENCES

Atkin, O.K., Zhang, Q., and Wiskich, J.T. (2002). Effect of temperature on rates of alternative and cytochrome pathway respiration and their relationship with the redox poise of the quinone pool. Plant Physiology **128,** 212-222.

Azzu, V., Jastroch, M., Divakaruni, A.S., and Brand, M.D. (2010). The regulation and turnover of mitochondrial uncoupling proteins. Biochimica et Biophysica Acta (BBA) - Bioenergetics **1797,** 785-791.

Balk, J., Leaver, C.J., McCabe, P.F. (1999)**.** Translocation of cytochrome c from the mitochondria to the cytosol occurs during heat-induced programmed cell death in cucumber plants. FEBS Letters **463,** 151-154

Bar-On, P., Mohsen, M., Zhang, R., Feigin, E., Chevion, M., Samuni, A. (1999) Kinetics of Nitroxide Reaction with Iron(II). Journal of the American Chemical Society **121**: 8070–8073

Barreto, P., Okura, V., Neshich, I.A., Maia, I.d., and Arruda, P. (2014). Overexpression of UCP1 in tobacco induces mitochondrial biogenesis and amplifies a broad stress response. BMC Plant Biology **14,** 144.

Bartlett, J.L., Levin, G., and Blount, P. (2004). An *in vivo* assay identifies changes in residue accessibility on mechanosensitive channel gating. Proceedings of the National Academy of Sciences of the United States of America **101,** 10161-10165.

Bass, R.B., Strop, P., Barclay, M., and Rees, D.C. (2002). Crystal structure of *Escherichia coli* MscS, a voltage-modulated and mechanosensitive channel. Science **298**, 1582-1587.

Beavis A.D. (1992). Properties of the inner membrane anion channel in intact mitochondria. Journal of Bioenergetics and Biomembranes **24**, 77-90.

Birke, H., Heeg, C., Wirtz, M., and Hell, R. (2013). Successful fertilization requires the presence of at least one major *O*-acetylserine(thiol)lyase for cysteine synthesis in pollen of Arabidopsis. Plant Physiology **163,** 959-972.

Booth, I.R., Rasmussen, T., Edwards, M.D., Black, S., Rasmussen, A., Bartlett, W., and Miller, S. (2011). Sensing bilayer tension: bacterial mechanosensitive channels and their gating mechanisms. Biochemical Society Transactions **39,** 733-740.

Clifton, R., Lister, R., Parker, K., Sappl, P., Elhafez, D., Millar, A.H., Day, D., and Whelan, J. (2005). Stress-induced co-expression of alternative respiratory chain components in *Arabidopsis thaliana*. Plant Molecular Biology **58,** 193-212.

Cox, C.D., Nomura, T., Ziegler, C.S., Campbell, A.K., Wann, K.T., and Martinac, B. (2013). Selectivity mechanism of the mechanosensitive channel MscS revealed by probing channel subconducting states. Nature Communications **4**, 2137.

Diolez, P., and Moreau, F. (1985) Correlation between ATP synthesis, membrane potential and oxidation rate in potato mitochondria. Biochimica et Biophysica Acta (BBA) - Bioenergetics **806**, 56-63.

Duncan, O., Carrie, C., Wang, Y., and Murcha, M. (2015). *In vitro* and *in vivo* protein uptake studies in plant mitochondria. In Plant Mitochondria, J. Whelan and M.W. Murcha, eds (Springer New York), pp. 61-81.

Edwards, M.D., Black, S., Rasmussen, T., Rasmussen, A., Stokes, N.R., Stephen, T.-L., Miller, S., and Booth, I.R. (2012). Characterization of three novel mechanosensitive channel activities in *Escherichia coli*. Channels **6,** 272-281.

Edwards, M.D., Bartlett, W., and Booth, I.R. (2008). Pore mutations of the *Escherichia coli* MscS channel affect desensitization but not ionic preference. Biophys. J. **94,** 3003-3013.

Escobar, M.A., Franklin, K.A., Svensson, Å.S., Salter, M.G., Whitelam, G.C., and Rasmusson, A.G. (2004). Light regulation of the Arabidopsis respiratory chain. Multiple discrete photoreceptor responses contribute to induction of type II NAD(P)H dehydrogenase genes. Plant Physiology **136,** 2710-2721.

Eubel, H., Jänsch, L., and Braun, H.-P. (2003). New insights into the respiratory chain of plant mitochondria. Supercomplexes and a unique composition of Complex II. Plant Physiology **133,** 274-286.

Ferro, M., Brugière, S., Salvi, D., Seigneurin-Berny, D., Court, M., Moyet, L., Ramus, C., Miras, S., Mellal, M., Le Gall, S., Kieffer-Jaquinod, S., Bruley, C., Garin, J., Joyard, J., Masselon, C., and Rolland, N. (2010). AT_CHLORO, a comprehensive chloroplast proteome database with subplastidial localization and curated information on envelope proteins. Molecular & Cellular Proteomics **9,** 1063-1084.

Fricker, M.D. (2016) Quantitative redox imaging software. Antioxidant and redox signalling **24**, 752-762

Froehlich, J.E., Wilkerson, C.G., Ray, W.K., McAndrew, R.S., Osteryoung, K.W., Gage, D.A., and Phinney, B.S. (2003). Proteomic study of the *Arabidopsis thaliana* chloroplastic envelope membrane utilizing alternatives to traditional two-dimensional electrophoresis. Journal of Proteome Research **2,** 413-425.

Gehl, B., Lee, C.P., Bota, P., Blatt, M.R., and Sweetlove, L.J. (2014). An Arabidopsis Stomatin-like protein affects mitochondrial respiratory supercomplex organization. Plant Physiology **164,** 1389-1400.

Hamilton, E.S., Schlegel, A.M., and Haswell, E.S. (2015a). United in diversity: Mechanosensitive ion channels in plants. Annual Review of Plant Biology **66,** 113-137.

Hamilton, E.S., Jensen, G.S., Maksaev, G., Katims, A., Sherp, A.M., and Haswell, E.S. (2015b). Mechanosensitive channel MSL8 regulates osmotic forces during pollen hydration and germination. Science **350,** 438-441.

Haswell, E.S., and Meyerowitz, E.M. (2006). MscS-like proteins control plastid size and shape in *Arabidopsis thaliana*. Current Biology **16,** 1-11.

Hensley, J.R., and Hanson, J.B. (1975). The action of valinomycin in uncoupling corn mitochondria. Plant Physiology **56,** 13-18.

Huang, S., Taylor, N.L., Whelan, J., and Millar, A.H. (2009). Refining the definition of plant mitochondrial presequences through analysis of sorting signals, N-terminal modifications, and cleavage motifs. Plant Physiology **150,** 1272-1285.

Huber, S.C., and Moreland, D.E. (1979). Permeability properties of the inner membrane of mung bean mitochondria and changes during energization. Plant Physiology **64,** 115-119.

Jezek, P., Costa, A.D.T., and Vercesi, A.E. (1997). Reconstituted plant uncoupling mitochondrial protein allows for proton translocation via fatty acid cycling mechanism. Journal of Biological Chemistry **272,** 24272-24278.

Jung, D.W., and Brierley, G.P. (1979). Swelling and contraction of potato mitochondria. Plant Physiology **64,** 948-953.

Kelso, G.F., Porteous, C.M., Coulter, C.V., Hughes, G., Porteous, W.K., Ledgerwood, E.C., Smith, R.A.J., and Murphy, M.P. (2001). Selective targeting of a redox-active ubiquinone to mitochondria within cells: Antioxidant and antiapoptotic properties. Journal of Biological Chemistry **276,** 4588-4596.

Kesseler, A., and Brand, M.D. (1994a). Effects of cadmium on the control and internal regulation of oxidative phosphorylation in potato tuber mitochondria. European Journal of Biochemistry **225,** 907-922.

Kesseler, A., and Brand, M.D. (1994b). Quantitative determination of the regulation of oxidative phosphorylation by cadmium in potato tuber mitochondria. European Journal of Biochemistry **225,** 923-935.

Kesseler, A., and Brand, M.D. (1994c). Localisation of the sites of action of cadmium on oxidative phosphorylation in potato tuber mitochondria using top-down elasticity analysis. European Journal of Biochemistry **225,** 897-906.

Klodmann, J., Senkler, M., Rode, C., and Braun, H.-P. (2011). Defining the protein complex proteome of plant mitochondria. Plant Physiology **157,** 587-598.

Kung, C., Martinac, B., and Sukharev, S. (2010). Mechanosensitive channels in microbes. Annual Review of Microbiology **64,** 313-329**.**

Kunz, H.H., Gierth, M., Herdean, A., Satoh-Cruz, M., Kramer, D.M., Spetea, C., and Schroeder, J.I. (2014) Plastidial transporters KEA1, -2, and -3 are essential for chloroplast osmoregulation, integrity, and pH regulation in Arabidopsis. Proceedings of the National Academy of Sciences of the United States of America **20**, 7480-7485.

Laus, M.N., Soccio, M., Trono, D., Cattivelli, L., Pastore, D. (2008) Plant Inner Membrane Anion Channel (PIMAC) function in plant mitochondria. Plant and Cell Physiology **49**, 1039-1055.

Lee, C.P., Eubel, H., O'Toole, N., and Millar, A.H. (2008). Heterogeneity of the mitochondrial proteome for photosynthetic and non-photosynthetic Arabidopsis metabolism. Molecular & Cellular Proteomics **7,** 1297-1316.

Levina, N., Tötemeyer, S., Stokes, N.R., Louis, P., Jones, M.A., and Booth, I.R. (1999). Protection of *Escherichia coli* cells against extreme turgor by activation of MscS and MscL mechanosensitive channels: identification of genes required for MscS activity. EMBO Journal **18,** 1730-1737.

Li, Y., Moe, P.C., Chandrasekaran, S., Booth, I.R., and Blount, P. (2002). Ionic regulation of MscK, a mechanosensitive channel from *Escherichia coli*. EMBO Journal **21**, 5323-5330.

Lin, T.-Y., and Markhart, A.H. (1990). Temperature effects on mitochondrial respiration in *Phaseolus acutifolius* A. Gray and *Phaseolus vulgaris* L. Plant Physiology **94,** 54-58.

Maksaev, G., and Haswell, E.S. (2012). MscS-Like10 is a stretch-activated ion channel from *Arabidopsis thaliana* with a preference for anions. Proceedings of the National Academy of Sciences of the United States of America **109,** 19015-19020.

Martinac, B., Rohde, P., Cranfield, C., and Nomura, T. (2013). Patch clamp electrophysiology for the study of bacterial ion channels in giant spheroplasts of *E. coli*. In Bacterial Cell Surfaces, A.H. Delcour, ed (Humana Press), pp. 367-380.

Millar, A.H., Sweetlove, L.J., Giegé, P., and Leaver, C.J. (2001). Analysis of the Arabidopsis mitochondrial proteome. Plant Physiology **127,** 1711-1727.

Miller, S., Bartlett, W., Chandrasekaran, S., Simpson, S., Edwards, M., and Booth, I.R. (2003). Domain organization of the MscS mechanosensitive channel of *Escherichia coli*. EMBO Journal **22,** 36-46.

Mitchell, P., and Moyle, J. (1969). Estimation of membrane potential and pH difference across the cristae membrane of rat liver mitochondria. European Journal of Biochemistry **7,** 471-484.

Møller, I.M. (2001). Plant mitochondria and oxidative stress: Electron transport, nadph turnover, and metabolism of reactive oxygen species. Annual Review of Plant Physiology and Plant Molecular Biology **52,** 561-591.

Moore, A.L., and Wilson, S.B. (1977). Translocation of some anions, cations, and acids in turnip (*Brassica napus l.*) mitochondria. Journal of Experimental Botany **28,** 607-618.

Moore, A.L., Shiba, T., Young, L., Harada, S., Kita, K., and Ito, K. (2013). Unraveling the heater: New insights into the structure of the alternative oxidase. Annual Review of Plant Biology **64,** 637-663.

Murcha, M.W., Lister, R., Ho, A.Y.Y., and Whelan, J. (2003). Identification, expression, and import of components 17 and 23 of the inner mitochondrial membrane translocase from Arabidopsis. Plant Physiology **131,** 1737-1747.

Murcha, M.W., Elhafez, D., Millar, A.H., and Whelan, J. (2004). The N-terminal extension of plant mitochondrial carrier proteins is removed by two-step processing: The first cleavage is by the mitochondrial processing peptidase. Journal of Molecular Biology **344,** 443-454.

Murphy, M.P., Smith, R.A.J. (2007) Targeting antioxidants to mitochondria by conjugation to lipophilic cations. Annual Review of Pharmacology and Toxicology **47**: 629–656

Naismith, J.H., and Booth, I.R. (2012). Bacterial mechanosensitive channels—MscS: Evolution's solution to creating sensitivity in function. Annual Review of Biophysics **41,** 157-177.

Nicholls, D.G. (1974). The influence of respiration and ATP hydrolysis on the proton-electrochemical gradient across the inner membrane of rat-liver mitochondria as determined by ion distribution. European Journal of Biochemistry **50,** 305-315.

Nikolovski, N., Rubtsov, D., Segura, M.P., Miles, G.P., Stevens, T.J., Dunkley, T.P.J., Munro, S., Lilley, K.S., and Dupree, P. (2012). Putative glycosyltransferases and other plant golgi apparatus proteins are revealed by LOPIT proteomics. Plant Physiology **160,** 1037-1051.

Pivetti, C.D., Yen, M.R., Miller, S., Busch, W., Tseng, Y.H., Booth, I.R., and Saier, M.H., Jr. (2003). Two families of mechanosensitive channel proteins. Microbiology and Molecular Biology reviews **67**, 66-85.

Quinlan, C.L., Gerencser, A.A., Treberg, J.R., and Brand, M.D. (2011). The mechanism of superoxide production by the antimycin-inhibited mitochondrial Q-cycle. Journal of Biological Chemistry **286,** 31361-31372.

Rasmusson, A.G., Soole, K.L., and Elthon, T.E. (2004). Alternative NAD(P)H dehydrogenases of plant mitochondria. Annual Review of Plant Biology **55,** 23-39.

Ridone, P., Nakayama, Y., Martinac, B. and Battle, A.R. (2015) Patch clamp characterization of the effect of cardiolipin on MscS of *E. coli*. European Biophysics Journal **44**, 567–76.

Rowe, I., Elahi, M., Huq, A., and Sukharev, S. (2013). The mechanoelectrical response of the cytoplasmic membrane of *Vibrio cholerae*. Journal of General Physiology **142**, 75-85.

Santo-Domingo, J., and Demaurex, N. (2012). The renaissance of mitochondrial pH. Journal of General Physiology **139,** 415-423.

Samuni, A., Krishna, C.M., Mitchell, J.B., Collins, C.R., Russo, A. (1990) Superoxide reaction with nitroxides. Free Radical Research Communications **9**: 241–9

Schnorf M, Potrykus I, Neuhaus G (1994) Microinjection technique: routine system for characterization of microcapillaries by bubble pressure measurement. Experimental Cell Research **210,** 260-267.

Schwacke, R., Schneider, A., van der Graaff, E., Fischer, K., Catoni, E., Desimone, M., Frommer, W.B., Flügge, U.-I., and Kunze, R. (2003). ARAMEMNON, a novel database for arabidopsis integral membrane proteins. Plant Physiology **131,** 16-26.

Schwarzländer, M., Dick, T.P., Meyer, A.J., and Morgan, B. (2015). Dissecting redox biology using fluorescent protein sensors. Antioxidants & Redox Signaling. In press

Schwarzländer, M., Logan, D.C., Johnston, I.G., Jones, N.S., Meyer, A.J., Fricker, M.D., and Sweetlove, L.J. (2012). Pulsing of membrane potential in individual mitochondria: A stress-induced mechanism to regulate respiratory bioenergetics in Arabidopsis. Plant Cell **24,** 1188-1201.

Schwarzländer, M., Fricker, M.D., Müller, C., Marty, L., Brach, T., Novak, J., Sweetlove, L.J., Hell, R., and Meyer, A.J. (2008). Confocal imaging of glutathione redox potential in living plant cells. Journal of Microscopy **231,** 299-316.

Smith, A.M.O., Ratcliffe, R.G., and Sweetlove, L.J. (2004). Activation and function of mitochondrial uncoupling protein in plants. Journal of Biological Chemistry **279,** 51944-51952.

Steinbacher, S., Bass, R.B., Strop, P., and Rees, D.C. (2007). Structures of the prokaryotic mechanosensitive channels MscL and MscS. In Mechanosensitive Ion Channels, Part A, O.P. Hamill, ed, pp. 1-24.

Sukharev, S. (2002). Purification of the small mechanosensitive channel of *Escherichia coli* (MscS): the subunit structure, conduction, and gating characteristics in liposomes. Biophysical Journal **83**, 290-298.

Sweetlove, L.J., Taylor, N.L., and Leaver, C.J. (2007). Isolation of intact, functional mitochondria from the model plant *Arabidopsis thaliana*. Methods in Molecular Biology **372,** 125-136.

Trono, D., Laus, M.N., Soccio, M., Alfarano, M., and Pastore, D. (2015) Modulation of Potassium Channel Activity in the Balance of ROS and ATP Production by Durum Wheat Mitochondria—An Amazing Defense Tool Against Hyperosmotic Stress. Frontiers in Plant Sciences **6**,1072.

Trnka, J., Blaikie, F.H., Logan, A., Smith, R.A.J., and Murphy, M.P. (2009). Antioxidant properties of MitoTEMPOL and its hydroxylamine. Free Radical Research **43,** 4-12.

Vásquez, V., Sotomayor, M., Cordero-Morales, J., Schulten, K., and Perozo, E. (2008). A structural mechanism for MscS gating in lipid bilayers. Science **321,** 1210-1214.

Veley, K.M., Marshburn, S., Clure, C.E., and Haswell, E.S. (2012). Mechanosensitive channels protect plastids from hypoosmotic stress during normal plant growth. Current Biology **22,** 408-413.

Veley, K.M., Maksaev, G., Frick, E.M., January, E., Kloepper, S.C., and Haswell, E.S. (2014). Arabidopsis MSL10 Has a regulated cell death signaling activity that is separable from its mechanosensitive ion channel activity. Plant Cell **26,** 3115-3131.

Vercesi, A.E., Borecký, J., Maia, I.d.G., Arruda, P., Cuccovia, I.M., and Chaimovich, H. (2006). Plant uncoupling mitochondrial proteins. Annual Review of Plant Biology **57,** 383-404.

Wagner, S., Behera, S., De Bortoli, et al., (2015) The EF-Hand Ca^{2+} binding protein MICU choreographs mitochondrial Ca^{2+} dynamics in Arabidopsis. Plant Cell **27,** 3190-3212

Wilson, M.E., Jensen, G.S., and Haswell, E.S. (2011). Two mechanosensitive channel homologs influence division ring placement in Arabidopsis chloroplasts. Plant Cell **23,** 2939-2949.

Wilson, M.E., Basu, M.R., Bhaskara, G.B., Verslues, P.E., and Haswell, E.S. (2014). Plastid osmotic stress activates cellular stress responses in Arabidopsis. Plant Physiology **165,** 119-128.

Wittig, I., Beckhaus, T., Wumaier, Z., Karas, M., and Schägger, H. (2010). Mass estimation of native proteins by blue native electrophoresis: Principles and practical hints. Molecular & Cellular Proteomics **9,** 2149-2161.

Zotova, L., Aleschko, M., Sponder, G., Baumgartner, R., Reipert, S., Prinz, M., Schweyen, R.J., and Nowikovsky, K. (2010). Novel components of an active mitochondrial K^+/H^+ exchange. Journal of Biological Chemistry **285,** 14399-14414.

Zybailov, B., Rutschow, H., Friso, G., Rudella, A., Emanuelsson, O., Sun, Q., and van Wijk, K.J. (2008). Sorting signals, N-terminal modifications and abundance of the chloroplast proteome. PLoS ONE **3,** e1994.

FIGURE LEGENDS

Figure 1. The subcellular localization of MSL1 in Arabidopsis. (A) CLSM image of mesophyll cells from transgenic plants stably over-expressing MSL1-GFP. GFP signal is pseudocolored green and chlorophyll fluorescence is pseudocolored red. Scale bar = 20 μm (B) CLSM image of a root hair from a plant stably over-expressing MSL1-GFP after incubation with MitoTracker Red. GFP signal is pseudocolored green and MitoTracker red is pseudocolored red. Scale bar = 2 μm (C) Immunoblotting of isolated mitochondria and mitochondrial peripheral and integral membrane fractions following sodium carbonate treatment. Proteins were separated on a blue-native PAGE and immunoblots were probed using a peptide antibody raised against MSL1. Roman numerals correspond to the locations of respiratory complexes and ATP synthase complex on a typical 1D-blue-native PAGE of Arabidopsis mitochondria. (D) In vitro import of radiolabelled MSL1 into isolated mitochondria. Import reaction was carried out under conditions that support protein uptake into mitochondria. p, precursor protein; i, processed intermediate; m, processed mature protein. (E) Sub-mitochondrial location of MSL1. Isolated mitochondria were treated with (+) or without (-) osmotic shock to produce mitoplasts, proteinase K to digest exposed peptides and triton (TX-100) to solubilize all membranes. Immunoblotting was then carried out using antibodies raised against MSL1, stomatin 2 (SLP2, inner membrane), voltage-dependent anion channel (VDAC, outer membrane) and cytochrome c (cyt c, intermembrane space).

Figure 2. Channel function of MSL1 when expressed in *E. coli.* (A) Representative trace of an inside-out patch from a giant Δ7 (MJF641) *E. coli* spheroplast expressing mature MSL1, at a transmembrane potential of -20 mV. Channels were opened by administering negative pressure (suction) through the patch pipette. O_1-O_3 indicate successive individual

channel openings. (B) The current-voltage curve for MSL1 at negative membrane potentials. The single channel conductance of MSL1, calculated as the slope of this I/V curve, is 1.2 nS. N = 17 patches. (C) The same patch shown in (A) subjected to high extreme transmembrane potentials, without added membrane tension. The asterisk indicates channels occasional openings and closures. The arrow indicates patch rupture. (D) Current-voltage properties of the MSL1 channel under symmetric (filled circles, data is the same as in panel B) and asymmetric (open circles) conditions. Arrow marks the reversal potential of MSL1 in asymmetric buffers.

Figure 3. Function of MSL1 during osmotic shock. (A) Osmotic-shock survival of *E. coli* expressing AtMSL1. Osmotic shock assay with wild type (Frag-1) or mscL- mscS- mscK- (MJF465) *E. coli* strains harboring the indicated constructs. Survival of cells subjected to a 500 mM hypo-osmotic downshock is presented as a percentage of the survival of unshocked cells. Data shown are the average of three different experiments and error bars indicate standard deviation. Asterisk indicates significant difference ($p < 0.01$) by Student's t-test. (B) CLSM image showing the maximum intensity projection of mitochondria isolated from Col-0 and *msl1-1* following osmotic treatments. Isolated mitochondria were labelled with membrane potential-independent fluorescent dye MitoTracker Green, and were then subjected to osmotic shock. Labelled mitochondria were visualized by confocal microscopy with at least 10 focal steps (z-stacks) of 0.2 µm. Scale bar = 1 µm. (C) Volume of isolated mitochondria from B. The volume of each mitochondrion was estimated on the basis of the maximum intensity projection-derived radius, with the assumption that every mitochondria visualized after all in vitro treatments remain perfectly spherical. Data shown are the average of three different experiments, with at least 200 mitochondria analysed per experiment, and error bars denotes standard deviation. Asterisk indicates significant difference ($p < 0.05$) between sucrose treatments but not between genotypes according to the two-way ANOVA analysis.

Figure 4. Effect of the loss of MSL1 on membrane potential of isolated mitochondria in different respiratory states (A) Representative confocal image of isolated mitochondria from Col-0, *msl1* and complemented line (*msl1*/gMSL1) incubated with minimal respiration buffer containing succinate to induce state II respiration and loaded with fluorophores TMRM and MTG. TMRM is false-colored red and MTG is false-colored green. Scale bar = 1 µm. (B-E) Frequency distribution of $\Delta\Psi_m$ (expressed as the ratio between log-transformed intensity of TMRM and MTG) of isolated mitochondria in the presence of: (B) succinate (state II respiration); (C) malate and pyruvate (state II respiration); (D) succinate and 0.5 mM ADP

(state III respiration); (E) succinate, 0.5 mM ADP and 1 µM oligomycin; MitoTEMPOLData shown are the average of at least four different experiments, with at least 500 mitochondria analysed per experiment, and error bars denotes standard error of the mean. Asterisk on each panel label indicates significant difference ($p < 0.01$ according to ANOVA and Tukey's post-hoc analysis) between Col-0 vs *msl1-1* and *msl1-1* vs *msl1-1*/gMSL1 (complemented line) in the mean of TMRM:MTG fluorescence ratio from at least four independent experiments.

Figure 5. Effect of MSL1 knockout on $\Delta\Psi_m$ pulsing of isolated mitochondria. TMRM and MTG-labelled mitochondria were energized either by succinate (State II respiration) (A, B) or succinate and ADP (State III respiration) (C, D) and the responses from these fluorophores in individual mitochondria over two minutes were monitored by confocal microscopy. MTG-normalized TMRM fluorescence intensity traces of five representative mitochondria (A, C) and ln (TMRM/MTG) frequency distribution of the population (B, D) from Col-0 (left), *msl1-1* (middle) and complemented line *msl1-1*/gMSL1 (right) are shown. Gaussian fits to the frequency distributions are shown as coloured lines (B, D) and where more than one Gaussian was fitted, the red line indicates the amalgamated fit and the green and blue lines the individual fits (B). The following statistics were extracted to quantify pulsing and membrane potential: (E) the coefficient of variation as a measure of pulsing amplitude; (F) the normalised TMRM fluorescence of state II mitochondria between pulses (the mean of the right hand peak in the frequency distributions); (G) the proportion of pulsing (calculated as the normalised area under the curve of the left hand peak in the frequency distribution plots and. Each of these statistics were derived from at least 100 mitochondria in three independent experiments. Error bars indicate standard error and asterisks denotes significant differences between the indicated pairs based on ANOVA and Tukey's post-hoc analysis. * = $p<0.05$; ** = $p<0.01$; *** = $p<0.001$.

Figure 6. Effect of ROS scavengers and antioxidants on membrane potential of state II mitochondria isolated from WT, *msl1-1* and *msl1-1*/gMSL1 plants. TMRM and MTG-labelled mitochondria isolated from the three genotypes were energised with succinate (state II) and the effect of addition of the indicated ROS scavengers and antioxidants on TMRM and MTG fluorescence monitored by confocal microscopy. Each measurement consisted of at least 100 mitochondria and was repeated 2-3 times. For each measurement, a frequency distribution of TMRM:MTG was plotted and two Gaussian curves fitted to the biomodal distribution. The mean TMRM:MTG value of the right-hand of the two peaks was calculated. Abbreviations: dTPP, decyl-triphenylphosphonium bromide; MnTMPyP manganese tetrakis(1-methyl-4-pyridyl)porphyrin pentachloride. Values are means ± standard error and

asterisks denotes significant differences between the indicated pairs based on ANOVA and Tukey's post-hoc analysis. * = p<0.05; ** = p<0.01; *** = p<0.001

Figure 7. Effect of absence of MSL1 on in vivo mitochondrial redox status during abiotic stress. (A) Representative ratiometric pseudocolored images of mito-roGFP2 in Col-0 and *msl1-1* roots treated with oligomycin and Cd^{2+}. roGFP2 fluorescence was measured for excitation at 405 nm and 488 nm, and the degree of oxidation is calculated based on the ratio between the intensities from the two excitations (405/408 ratio) and the calibration of the probe using 10 mM DTT and 10 mM H_2O_2. The colour scale represents the redox state of roGFP2 ranging from fully reduced in indigo to fully oxidized in red. Scale bar = 50 µm. (B) Quantitation of mito-roGFP2 oxidation state in Col-0 and *msl1-1* roots treated with respiratory inhibitors. Concentration of inhibitors used: 10 µM oligomycin A, 20 µM antimycin A, 20 µM rotenone, 1 mM sodium ascorbate, 1 mM propranolol 25 µM carbonyl cyanide m-chlorophenyl hydrazone (CCCP). (C) Quantitation of mito-roGFP2 oxidation state in Col-0 and *msl1-1* roots under abiotic stress conditions. All treatments were carried out in the dark for 1 hr in ½MS medium (pH 5.7) unless otherwise stated. At least 10 seedlings in several independent experiments were examined, with error bars indicate standard error. "a" and "b" indicate significant difference ($p < 0.01$ based on ANOVA and Tukey post-hoc analysis), respectively, between Col-0 and *msl1-1* under the same treatment and between control and treatment.

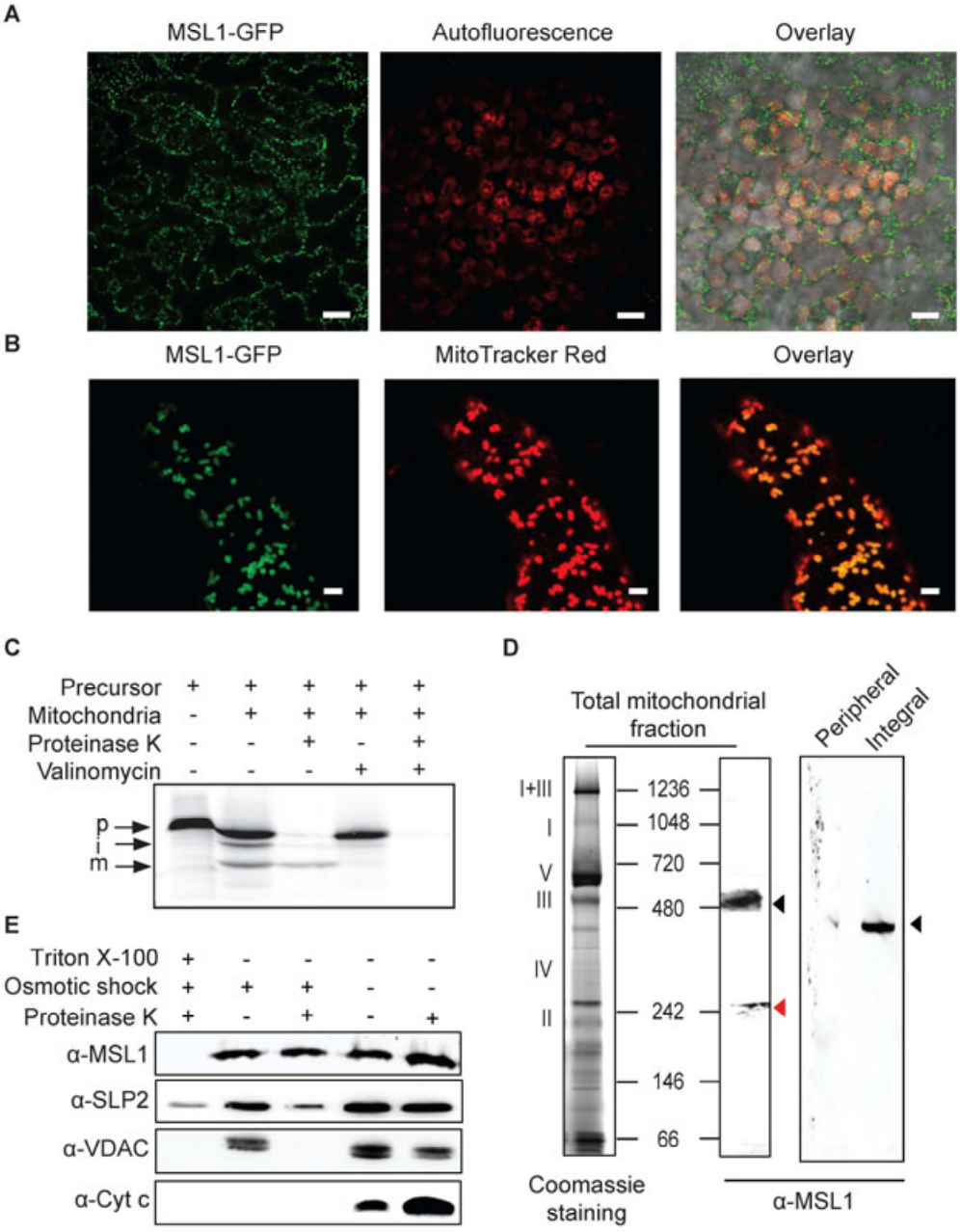

Figure 1. Subcellular localization of MSL1 in Arabidopsis.

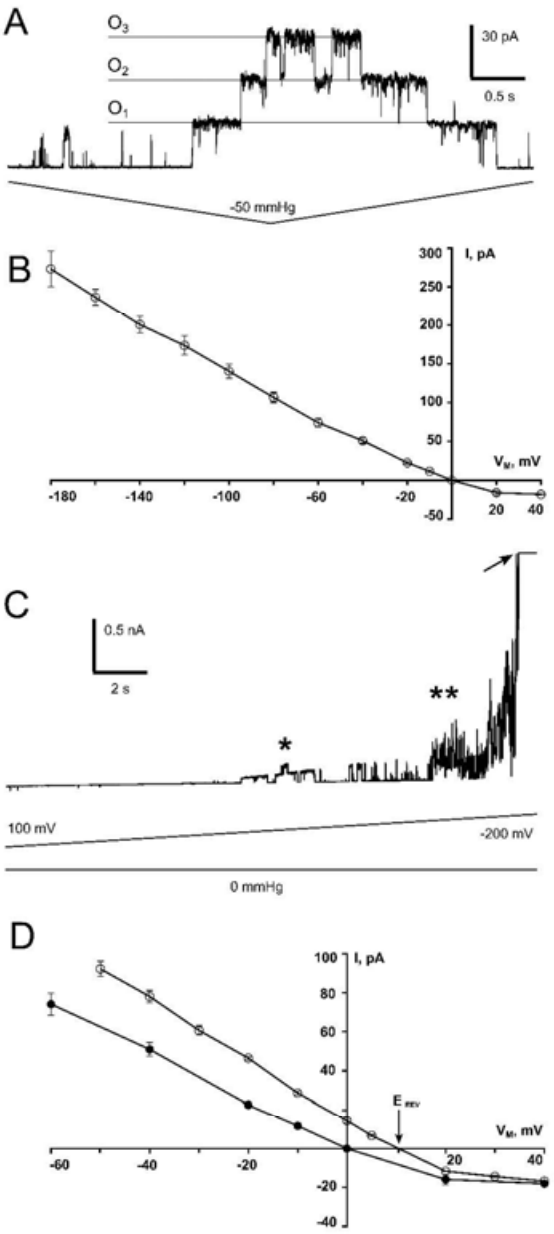

Figure 2. Channel function of MSL1 when expressed in *E. coli*.

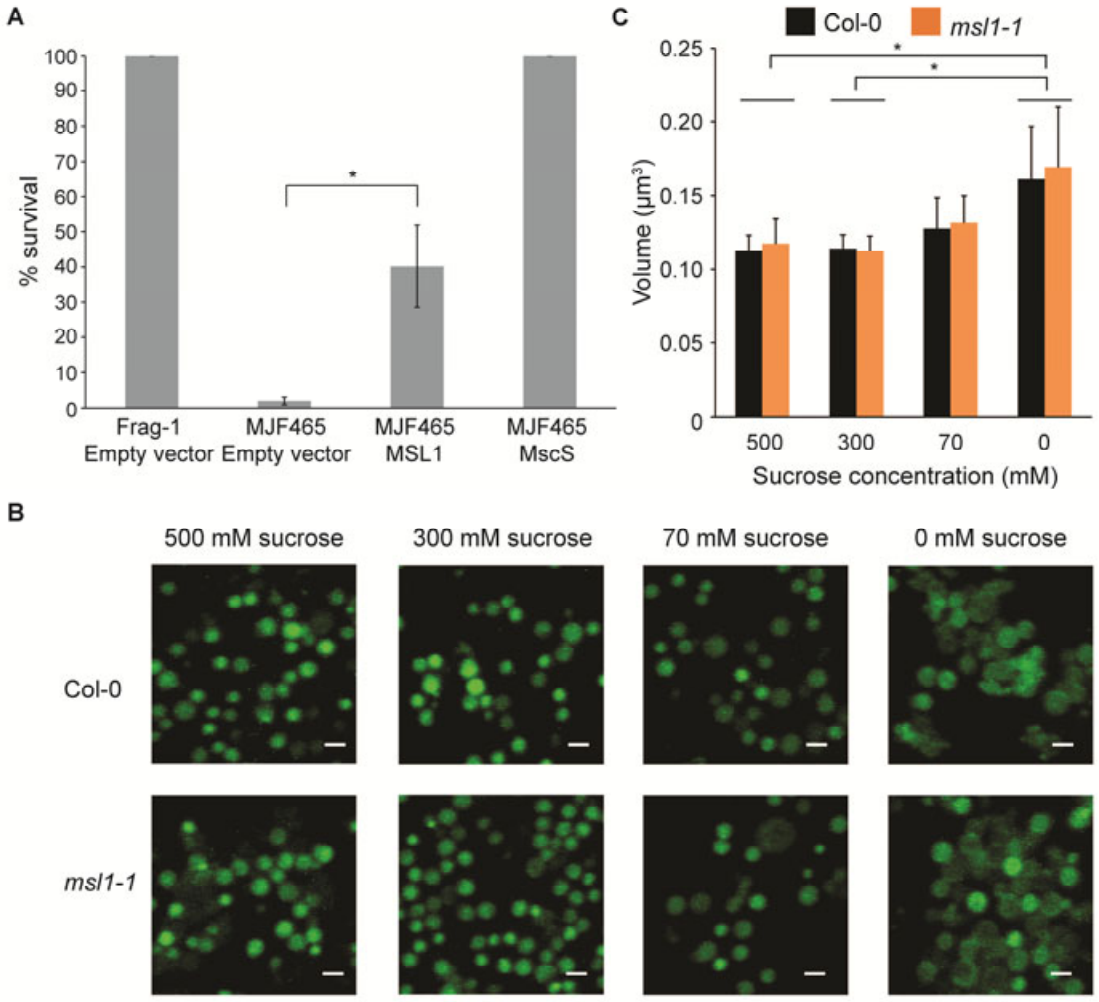

Figure 3. Function of MSL1 during osmotic shock

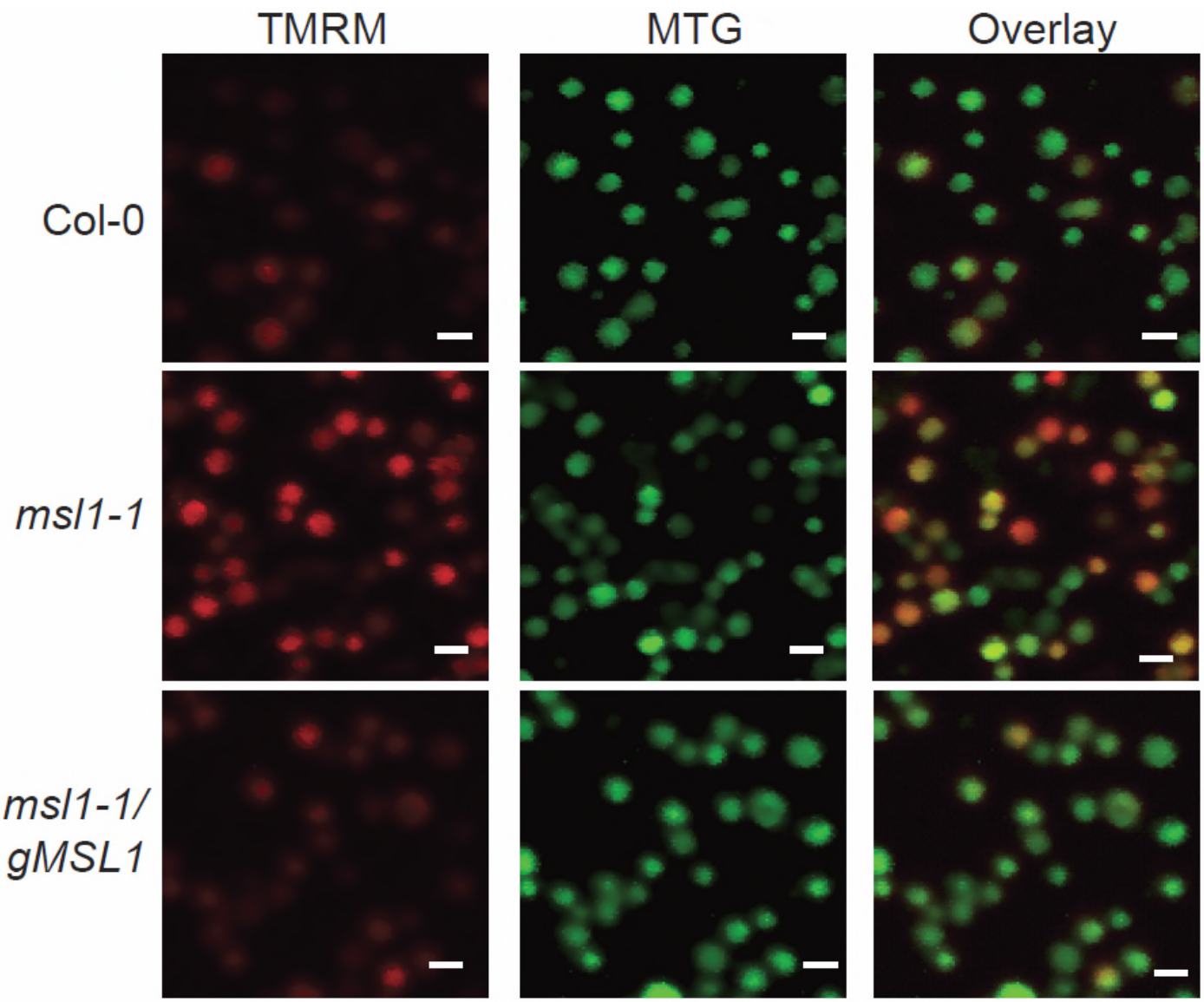

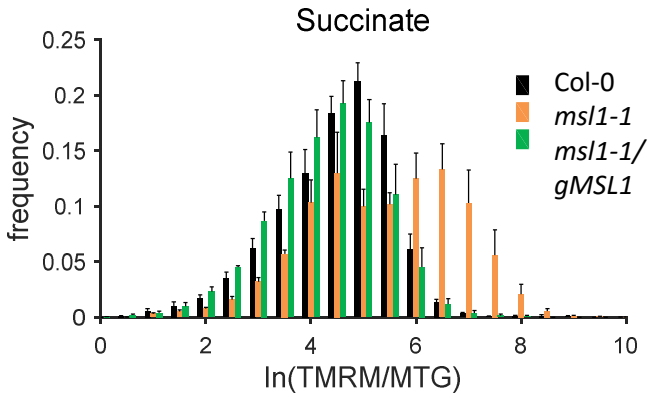

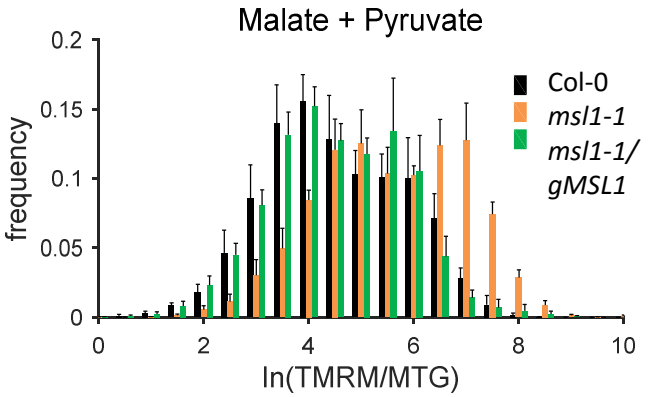

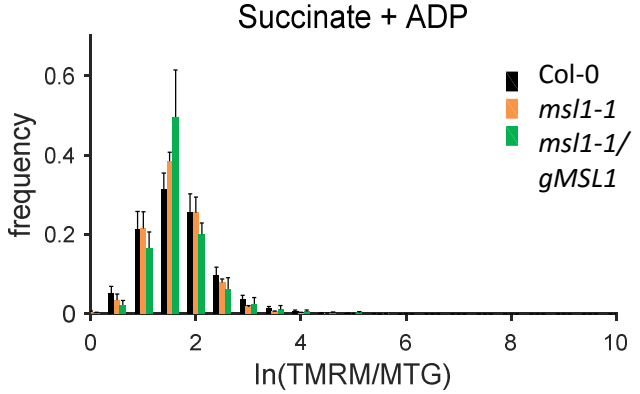

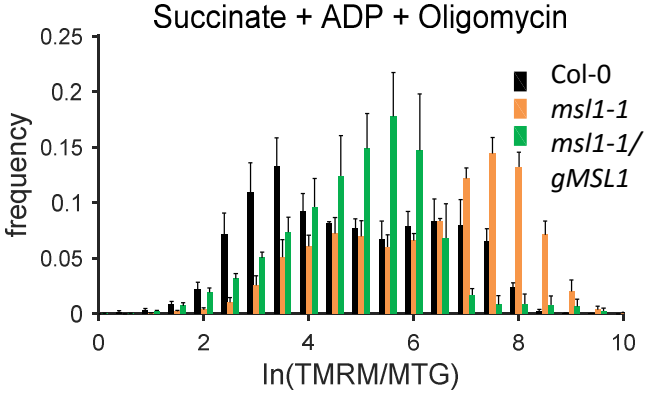

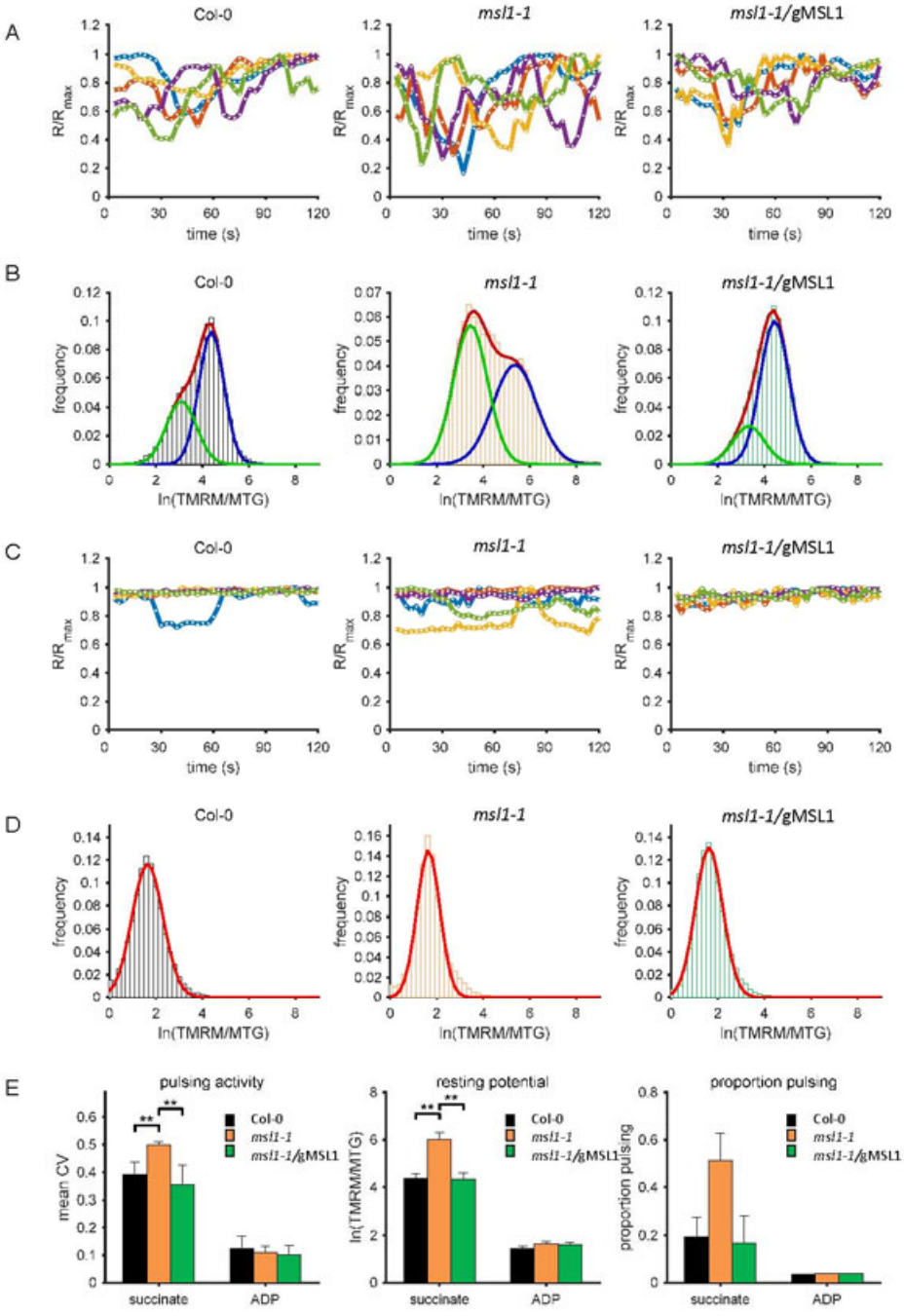

Figure 5. Effect of MSL1 knockout on $\Delta\Psi_m$ pulsing of isolated mitochondria.

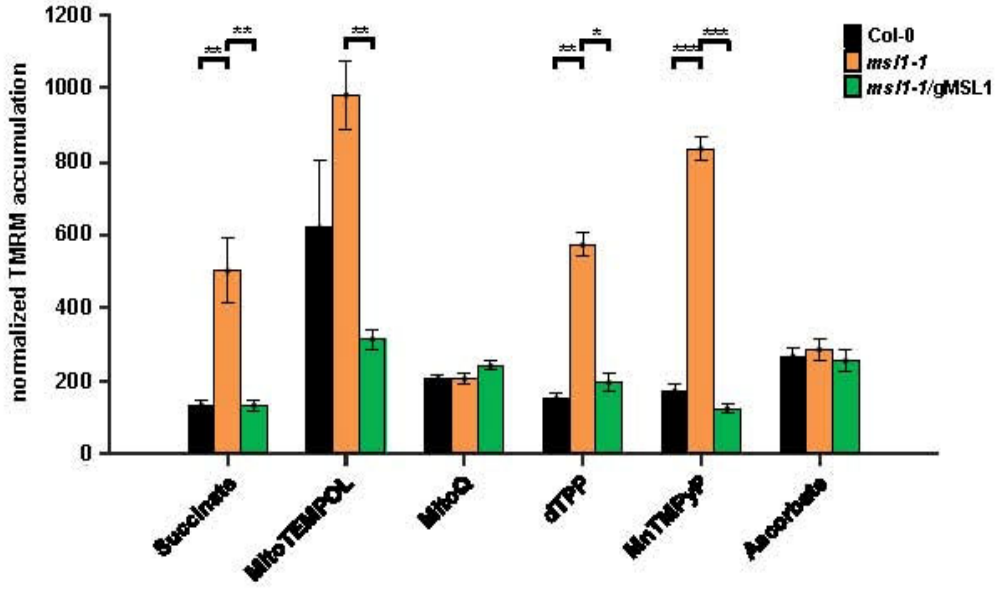

Figure 6. Effect of ROS scavengers and antioxidants on membrane potential of state II mitochondria isolated from WT, *msl1* and *msl1*/gMSL1 plants.

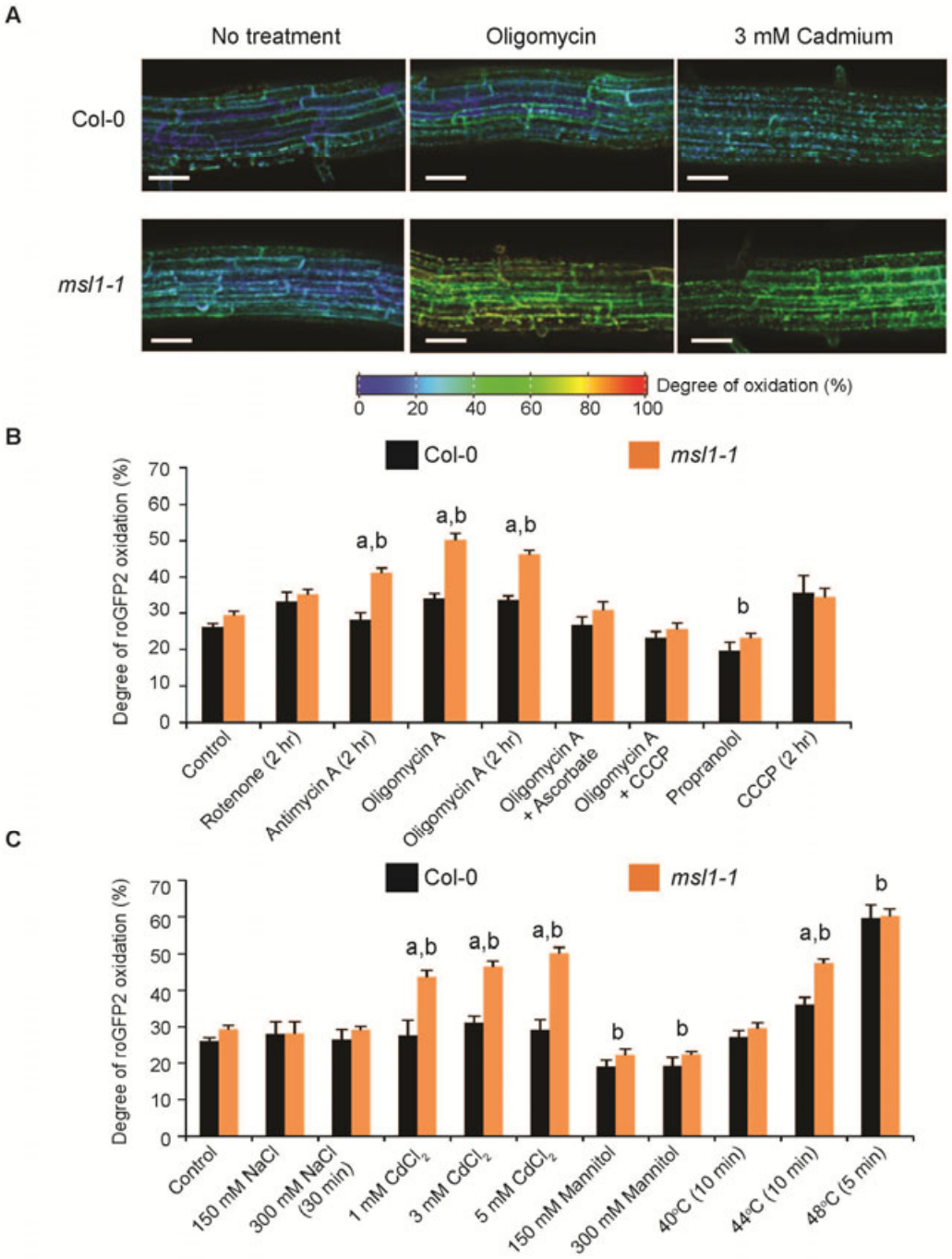

Figure 7. Effect of absence of MSL1 on in vivo mitochondrial redox status during abiotic stress.